工學碩士 學位論文

스퍼터링을 이용한 고품질 AlN 박막 성장과 평가

Growth and evaluation of high quality AlN using sputtering

指導敎授 張志豪
共同指導敎授 李文鎭

2018 年 2 月

韓國海洋大學校 大學院

海洋科學技術融合學科

趙 成 珉

본 논문을 조성민의 공학석사 학위논문으로 인준함

위원장   안 지 훈   (인)

위   원   장 지 호   (인)

위   원   윤 중 한   (인)

2018年   1月

한국해양대학교 해양과학기술전문대학원

Contents

3. Reactive Gas DC magnetron Sputtering of AlN thin films

4. Pulsed Sputtering Deposition of AlN Thin Films

5. Characterizations of AlN Thin Films

6. Conclusion ·································· 75

List of Tables

List of Figures

List of Figures

List of Figures

스퍼터링을 이용한 고품질 AlN 박막 성장과 평가

Sungmin Cho

Department of Convergence Study on the Ocean Science and Technology

Graduate School of Korea Maritime and Ocean University

Abstract

넓은 밴드갭, 높은 열전도도와 표면 탄성 속도와 같은 우수한 물성을 지니고 있는 AlN (질화 알루미늄)은 다양한 분야에 활용되고 있다. 지금까지는 AlN 박막은 주로 MOCVD, MBE 및 스퍼터 등과 같은 박막 성장 장비들을 이용하여 성장하였다. 하지만 스퍼터로 제작된 AlN 박막은 저온 성장의 가능성, 박막의 낮은 거칠기 및 낮은 제조 단가와 같은 장점이 있지만 결정성의 관점에서는 특정 용도로서 활용에는 충분하지 않았다. 스퍼터된 AlN 박막의 결정성은 스퍼터링 조건들에 영향을 받는 것으로 보고된다. 그러므로 스퍼터링 방법으로 고품질의 AlN 박막을 제조하기 위해서는 스퍼터링 조건이 AlN 박막에 미치는 영향에 관한 연구가 필요하다. 본 연구에서는 AlN 박막의 응용 확대를 위해, 스퍼터링을 이용하여 AlN 박막의 성장과 평가에 관한 연구를 하였다.

1장에서는 이 연구의 배경과 동기에 대해 소개하였다. AlN의 결정 구조, 특성, 응용 분야 및 AlN 박막을 제작하기 위한 방법들을 서술하였다.

2장에서는 실험에 사용한 장비에 대해 기술하였다. AlN 박막의 제조를 위한 스퍼터링 방법들과 XRD, SEM, EDS, AFM, CL과 같은 AlN 박막의 분석 및 평가를 실시한 장비들을 설명하였다.

3장에서는 DC 반응성 가스 마그네트론 스퍼터를 이용하여 AlN 박막의

성장에 대해 설명하였다. 박막들은 공급량의 변화에 따라 화학양론적 조성의 변화에 대한 관점으로 결정성에 미치는 영향에 대해 연구하였다.

4장에서는 펄스 스퍼터를 이용하여 AlN 박막에 성장에 대해 연구하였다. 3장의 내용을 활용하여 AlN 박막의 성장 조건 최적화를 실시하였다.

5장에서는, 다양한 분야의 활용 가치를 판단하기 위해, 4장에서 최적화된 AlN 박막의 물성을 평가하였다.

마지막으로 6장에서 모든 결과를 요약하고 본 연구의 결론을 설명 하였다.

KEY WORDS: 질화 알루미늄, Pulsed DC reactive magnetron sputtering, 화학양론적 조성, 잔류 스트레인, 결정성, 전기적 특성, 광학적 특성

Growth and evaluation of high quality AlN using sputtering

Sungmin Cho

Department of Convergence Study on the Ocean Science and Technology

Graduate School of Korea Maritime and Ocean University

Abstract

AlN (aluminum nitride), which has excellent properties such as wide band gap, high thermal conductivity and surface acoustic velocity, is utilized in various fields. Up to now, AlN thin films are mainly grown using thin film growth equipments such as MOCVD, MBE and sputter. However, AlN thin films fabricated by sputtering have advantages such as a higher possibility of a low temperature growth, a low roughness of thin film and a low manufacturing cost, but it is not satisfying in terms of crystallinity for certain applications. It was reported that the crystallinity of the sputtered AlN thin film is affected by the sputtering conditions. Therefore, in order to fabricate high-quality AlN thin films by sputtering, it is necessary to study the influence of sputtering conditions on AlN thin films. In this study, I researched the growth and evaluation of AlN thin films by sputtering for the widen application of AlN thin films.

In the chapter 1, the background and motivation of this study were introduced. The crystal structure, properties, application fields of AlN and methods for fabricating AlN thin films were described.

In the chapter 2, the equipments used in the experiment were introduced. The sputtering methods for fabrication of AlN thin film and

equipments for the analysis and evaluation of AlN thin films such as XRD, SEM, EDS, AFM, and CL are described.

In the chapter 3, The growth of AlN thin films was demonstrated using a DC reactive gas magnetron sputter. The Influences to the crystallinity in terms of the stoichiometric composition change with changes of the supply amount were investigated.

In the chapter 4, The growth of the AlN thin film is discussed using a pulsed sputter. The growth conditions of the AlN thin film are optimized by utilizing the content of chapter 3.

In chapter 5, In order to evaluate the utilization value of various fields, the physical properties of the optimized AlN thin films were evaluated in chapter 4.

Finally, In the chapter 6 all results are summarized and conclusions of this study were explained.
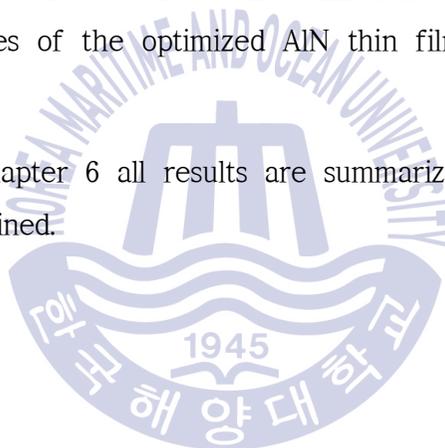
KEY WORDS: Aluminum nitride (AlN), Pulsed DC reactive magnetron sputtering, Stoichiometric composition, Residual strain, Crysatllinity, Electrical property, Optical property

Chapter 1. Introduction

1.1 Aluminum nitride

1.1.1 Crystal structure

Aluminium nitride (AlN) is one of a group of Ⅲ-Ⅴ nitride semiconductor such as gallium nitride (GaN), indium nitride (InN) and boron nitride (BN). Figure 1.1 shows the representatively reported wurtzite structure of AlN. The lattice constant is reported as a-axis = 3.111Å and c-axis = 4.979Å (PDXL: no. 00-025-1133). Because of instability and ionicity of lattice, the c/a ratio of 1.6 is changed from ideal wurtzite crystal structure. [1] Each Al atom (N atom) is surrounded by four N atoms (Al atoms) of tetrahedral site as shown in Figure 1.1 (b). The length between Al and N1 is 1.917Å (B1 bond) and Al to N2 is 1.885Å. (B2 bond) The angle of N1-Al-N3 is 107.7° and N2-Al-N3 is 110.5°. The bonding energy of B2 is relatively larger than it of B1. AlN(10-10) is only composed of the B1 bond, while AlN(0002) and AlN(11-20) is consisted of both bond B1 and B2. Therefore high energies of adatoms are required for growth of AlN (0002) thin film using sputtering [2].

In addition, AlN also has other crystal structures such as metastable cubic zinc-blend structure (z-AlN) and the high pressure cubic rock salt structure (r-AlN). z-AlN and r-AlN have the lattice parameter a = 4.83Å and a = 4.043~4.045Å at room temperature, respectively. N. Li, et al. has reported about other crystal structures experimentally and using density functional theory. [3]
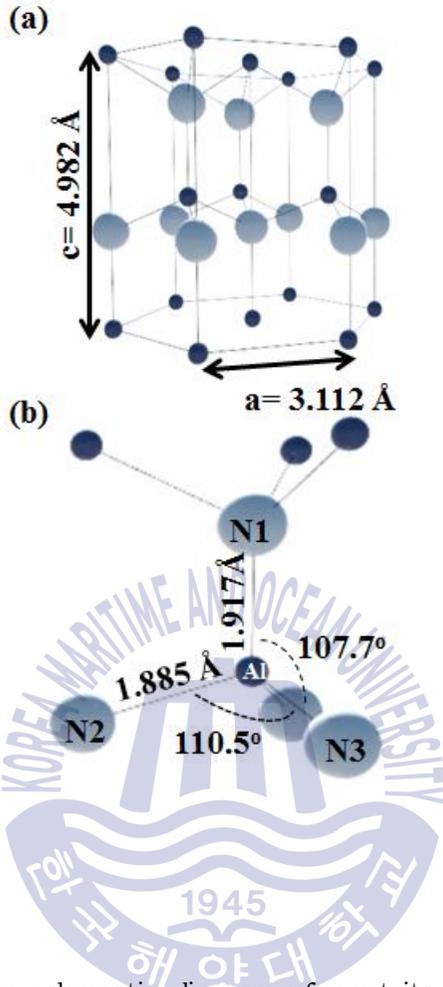
Figure 1.1 The schematic diagram of wurtzite AlN structure

1.1.2 Physical properties

Table 1.1 The physical properties of wurtzite aluminum nitride

Energy gap	$E_g(300K)$= 6.2eV
Index of Refraction	n(3eV)=2.15, n(3.42eV)=2.85
Melting point	2500K
Thermal expansion	$\triangle$a/a = 4.2×10^{-6}/K
Thermal conductivity	k=319 W/m·K
Hardness	17.7 GPa
Toughness	0.4 MPa·$m^{1/2}$
Young's modulus	308 Gpa
Relative permittivity	8.5 at 1MHz
Resistivity	$10^9 - 10^{11}$ Ωm

AlN is well known as a hard material having 9 at mohs' scale and chemically stable material. The mechanical properties of c-axis oriented AlN is reported as hardness of 17.7 GPa, fracture toughness of 0.4 MPa·$m^{1/2}$ and Young's modulus of 308 Gpa at room temperature (RT) [4]. However, it is softer than 6H-SiC (0001) of 22.9 GPa and α-Al_2O_3 (0001) of 28 GPa [5] and harder than GaN (0001) of 10.2GPa [6].

AlN is stable at high temperature (melting point : ~2500K). The thermal conductivity of pure AlN is 319 Wm·K^{-1} at RT [7]. Also thermal expansions of a-axis ($\triangle$a/a_0) and c-axis ($\triangle$c/c_0) are changed as following equation 1.1 and equation 1.2, respectively. [8]

$$\triangle a/a_0 = -8.68\times10^{-2} + 1.93\times10^{-4}T + 3.40\times10^{-7}T^2 - 7.97\times10^{-11}T^3 \qquad (1.1)$$

$$\triangle c/c_0 = -7.01\times10^{-2} + 1.58\times10^{-4}T + 2.72\times10^{-7}T^2 - 5.83\times10^{-11}T^3 \qquad (1.2)$$

The optical properties such as fundamental band gap of AlN were reported by Yamashita et al. at 1979. [9] It has optical properties of wide direct band gap (6.2eV) at RT and high optical transmittance at visible wavelength.

Also AlN has high electrical resistivity (10^9 – 10^{11} Ωm) [10] and dielectric constant (8.5 at 1MHz) [11] and has high surface acoustic velocity of 5.76km/s [12].

1.1.3 Applications

Due to the properties mentioned in chapter 1.1.2, AlN thin films has various applications as illustrated in figure 1.2.

In applications of optoelectronics, AlN thin films is well known as buffer layer between Si and GaN for relaxation of thermal expansion and lattice misfit [13]. It inhibits etching of Si layer from Ga called melt-back reaction [14]. Also the wide direct band gap (6.2eV) of AlN makes it can be adopted for deep-ultraviolet (DUV) LED [15]. However, for the expansion of optoelectrionic applications, it is needed to apply acceptor doping and activation of p-tpye AlN.

In applications of power electronics packaging, AlN-based micro-channel heat sink (MCHS) has been investigated. [16] Shan Yin et al. have reported that AlN is regarded as promising material due to thermal conductivity and high mechanical strength. It has similar lattice parameter and coefficient of thermal expansion (CTE) compared to SiC substrate using in power electronics.

AlN thin films have been attracting attention for application of surface acoustic wave (SAW) devices and bulk acoustic wave resonators (FBARs). A basic structure of SAW sensor is consisted of two interdigitated transducers (IDT) on piezoelectric films and space called the delay-line between the input and output IDT. The micro mass variation caused in delay-line makes the difference of each frequency detected at input and output IDT. It is important for c-axis oriented AlN thin films to have low roughness for SAW device and FBARs for piezoelectric constant and electricity coupling coefficients required for minimizing frequency variations caused by local

velocity changes. The SAW characteristics were utilized for as sensor [17] and filter [18].

AlN was studied for resistive switching (RS) materials such as capacitance of transparent MIM (Metal-Insulator-Metal) structure [19] and high electron mobility transistors (HEMTs) of MIS (Metal-Insulator-Semiconductor) structure [20]. RS materials based on nitride semiconductor are known for a high thermal conductivity, good insulating property, wide optical band gap and featured low voltage/current operation [19].
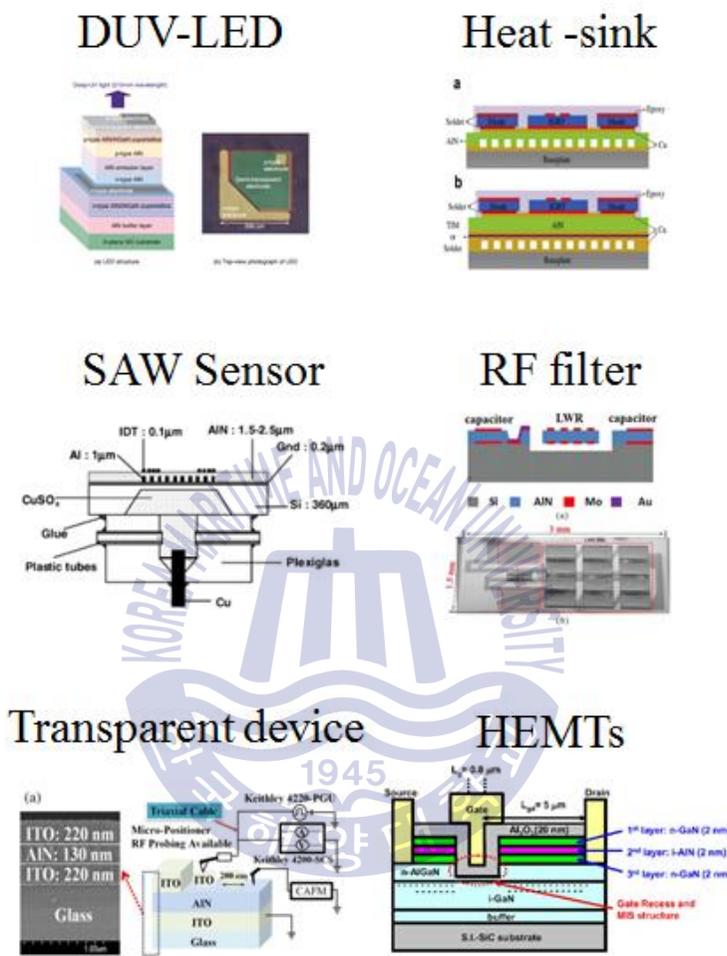
Figure 1.2 The schematics of AlN thin films of applications such as DUV-LED [15], Heat-sink [16], SAW sensor [17], RF filter [18], transparent device [19] and HEMTs [20]

1.2 Growth methods for AlN thin films

The AlN films has been grown using conventional growth methods MOCVD [21] and MBE [22]. The methods are generally required growth at high temperatures (above 950°C) to supply source for the growth of AlN films. However, It is possible that AlN thin films of high quality is fabricated. The lower crystal quality has been reported using sputter. However, it has benefits of low growth temperature, low price and low roughness of AlN thin films. [23] Therefore, sputtered AlN thin films is needed for widening application fields.

In order to maximize the advantages of sputtered AlN thin films, sputtering parameters such as cathode, anode and chamber were investigated for improving crystallinity of AlN thin film. The gas pressure [24] and Ar/N_2 gas flow ratio [25] were controlled as chamber parameter. The controlled parameter of cathode with target involves plasma power [26] and pulsed frequency/off time [27]. The controlled parameters of anode with substrate are substrate temperature and substrate bias. [28] The distance between cathode and anode is controlled. [29] Through them, it can be seen that the sputtering parameters affect crystallinity of AlN thin films.

1.3 Outline of thesis

In this study, AlN thin films were grown and evaluated using sputter to expand the field of applications. Sputtering parameters such as plasma power, gas flow ratio, substrate temperature and gas flow ratio are controlled for enhancing crystallinity of AlN thin films.

In chapter 3, the fundamental growth principle of the reactive gas DC magnetron sputtering method for the growth of AlN thin films were described.

In chapter 4, utilizing influences of sputtering condition which mentioned chapter 3, the growth conditions of AlN thin films by using pulsed sputtering deposition is optimized.

In chapter 5, The feasibility of AlN thin film is evaluated for widen applications.

Reference

[1] Borom, M. P., Slack, G. A. & Szymaszek, J. W., 1972. Thermal conductivity of commercial aluminum nitride, *American Ceramic Society Bulletin,* 51(11), pp.852-856.

[2] Zhang, J. X. et al., 2005. Growth of AlN films on Si (100) and Si (111) substrates by reactive magnetron sputtering. *Surface and Coatings Technology*, 198(1-3), pp.68-73.

[3] Li, N. et al., 2016. Growth and Stress-induced Transformation of Zinc blende AlN Layers in Al-AlN-TiN Multilayers. *Scientific Reports,* 5(1). pp.1-7.

[4] Yonenaga, I., Nikolaev, A., Melnik, Y., & Dmitriev, V., 2001. High-Temperature Hardness of Bulk Single-Crystal AlN. *Japanese Journal of Applied Physics,* 40(Part 2, No. 5A), pp.L426-L427.

[5] Farber, B. Y., Yoon, S. Y., Lagerlöf, K. P. D., & Heuer, A. H., 1993. Microplasticity during High Temperature Indentation and the Peierls Potential in Sapphire (α-Al$_2$O$_3$) Single Crystals. *Physica Status Solidi (a),* 137(2), pp.485-498.

[6] Yonenaga, I., Hoshi, T., & Usui, A., 2000. Hardness of Bulk Single-Crystal Gallium Nitride at High Temperatures. *Japanese Journal of Applied Physics,* 39(Part 2, No. 3A/B), pp.L200-L201.

[7] Slack, G. A., Tanzilli, R. A., Pohl, R. O., & Vandersande, J. W., 1987. The intrinsic thermal conductivity of AlN. *Journal of Physics and Chemistry of Solids*, 48(7), pp.641-647.

[8] Hull, R., Osgood, R. M., & Sakaki, H., 1999. *Nitride Semiconductors and Devices.* Springer:Berlin Heidelberg.

[9] Yamashita, H., Fukui, K., Misawa, S., & Yoshida, S., 1979. Optical

properties of AlN epitaxial thin films in the vacuum ultraviolet region. *Journal of applied physics*, 50, pp.896-898

[10] Kumari, N., Singh, A. K., & Barhai, P. K., 2014. Study of Properties of AlN Thin Films Deposited by Reactive Magnetron Sputtering. *International Journal of Thin Films Science and Technology,* 3(2), pp.43-49.

[11] Levinshtein, M. E., Rumyantsev, S. L., & Shur, M. (Eds.)., 2001. *Properties of advanced semiconductor materials: GaN, AlN, InN, BN, SiC, SiGe.* Wiley:New York.

[12] Bu, G. et al., 2006. Surface acoustic wave velocity in single-crystal AlN substrates. IEEE Transactions on Ultrasonics, *Ferroelectrics and Frequency Control*, 53(1), pp.251-254.

[13] Amano, H. et al., 1988. Effects of the buffer layer in metalorganic vapour phase epitaxy of GaN on sapphire substrate. *Thin Solid Films,* 163, pp.415-420.

[14] Ishikawa, H. et al., 1998. Thermal stability of GaN on (111) Si substrate. *Journal of Crystal Growth*, 189-190, pp178-182.

[15] Taniyasu, Y., & Kasu, M., 2008. Aluminum nitride deep-ultraviolet light-emitting p-n junction diodes. *Diamond and Related Materials,* 17(7-10), pp.1273-1277.

[16] S. Yin, Tseng, K., & Zhao, J., 2013. Design of AlN-based micro-channel heat sink in direct bond copper for power electronics packaging. A*pplied Thermal Engineering*, 52, pp.120-129.

[17] Duhamel, R. et al., 2006. Sensitivity of a Lamb wave sensor with 2μm AlN membrane. *Ultrasonics*, 44, pp.e893-e897.

[18] Liang, J. et al., 2015. Lamb Wave AlN Micromechanical Filters

Integrated With On-chip Capacitors for RF Front-End Architectures. *IEEE Journal of the Electron Devices Society*, 3, pp.361-364.

[19] Kim, H.-D., An, H.-M., Seo, Y., & Kim, T. G., 2011. Transparent Resistive Switching Memory Using ITO/AlN/ITO Capacitors. *IEEE Electron Device Letters*, 32(8), pp.1125-1127.

[20] Kanamura, M. et al., 2010. Enhancement-Mode GaN MIS-HEMTs With n-GaN/i-AlN/n-GaN Triple Cap Layer and High- k Gate Dielectrics. *IEEE Electron Device Letters,* 31(3), pp.189-191.

[21] Chen, Y. et al., 2014. Influence of the growth temperature of AlN nucleation layer on AlN template grown by high-temperature MOCVD. Material Letter 114, pp.26-28.

[22] Fan, Z. Y. et al., 2000. MBE Growth and Ultrahigh Temperature Processing of High-Quality AlN Films. *Materials Research Society Symposium*, 587, pp.07.12.1-07.12.6.

[23] Kumari, N., Singh, A. K., & Barhai, P. K., 2014. Study of Properties of AlN Thin Films Deposited by Reactive Magnetron Sputtering. *International Journal of Thin Films Science and Technology,* 3(2), pp.43-49.

[24] Ohtsuka, M., Takeuchi, H., & Fukuyama, H., 2016. Effect of sputtering pressure on crystalline quality and residual stress of AlN films deposited at 823 K on nitrided sapphire substrates by pulsed DC reactive sputtering. *Japan Society of Applied Physics*, 55, 05FD08.

[25] Iqbal, A., Walker, G., Iacopi, A., & Mohd-Yasin, F., 2016. Controlled sputtering of AlN (002) and (101) crystal orientations on epitaxial 3C-SiC-on-Si (100) substrate. *Journal of Crystal Growth*, 440, pp.76-80.

[26] Takeuchi, H., Ohtsuka, M., & Fukuyama H., 2015. Effect of sputtering power on surfacecharacteristics and crystal quality of AlNfilms deposited

by pulsed DC reactive sputtering. *Phys. Status Solidi B*, 252(5), pp.1163-1171.

[27] Cherng J. S., & Chang D. S., 2010. Effects of pulse parameters on the pulsed-DC reactive sputtering of AlN thin films. *Vacuum*, 84, pp.653-656.

[28] Barshilia, H. C., Deepthi, B., & Rajam K.S., 2008. Growth and characterization of aluminum nitride coatings prepared by pulsed-direct current reactive unbalanced magnetron sputtering. *Thin Solid Films*, 516, pp. 4168-4174.

[29] Iriarte, G. F., Rodriguez, J. G., & Calle, F., 2011. Effect of substrate-target distance and sputtering pressure in the synthesis of AlN thin films. *Microsystem Technologies* 17(3) pp.381-386
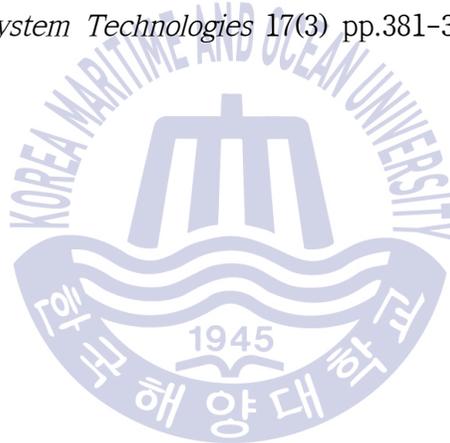
Chapter 2. Experimental Equipment

2.1 Sputter

Sputter technique is generally classified as one of physical vapor deposition (PVD) in thin films growth method. It is a method of depositing atoms formed from the target on a substrate and it happens when the ionized particles collide with the target at a low pressure (<5 mTorr). Figure 2.1 shows the fundamental sputter mechanism. A brief concept of the mechanism is supplying power between target (cathode) and substrate (anode) at a low pressure (typically range : few mtorr). Ions can be generated by the collision of high energy electrons with neutral atoms according to the equation. 2.1.

$$Ar + e^- \,(primary) = Ar^+ + e^- \,(primary) + e^- \,(secondary) \tag{2.1}$$

Plasma is formed at discharged area. When ionized atoms accelerate and collide with the target, the newly generated atoms from the surface of the aiming material under the condition that the collision energy is greater than the bonding energy of the material surface.

The sputtering method of AlN films brings benefits in diverse ways such as a low temperature growth, a smooth surface, and a low cost. According to the study, however, the crystal quality of sputtered AlN is still not meeting the demands of the certain fields.
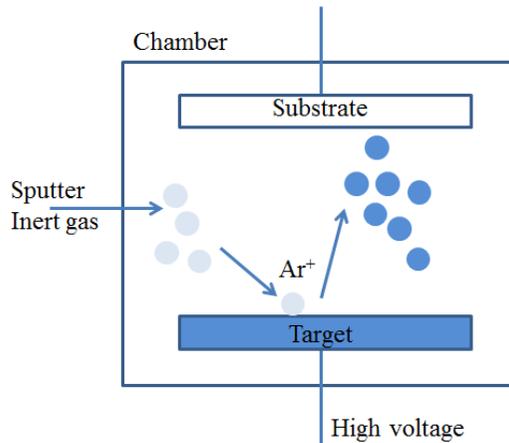
Figure 2.1 The schematic of sputtering process

2.1.1 DC discharge

The direct current (DC) discharge in sputtering process can be divided into dark discharge, glow discharge, arc discharge depending on the voltage and current to be formed as shown figure 2.2.

A dark discharge is invisible eye except for corona discharges and the breakdown. Townsend regime with exponentially increasing current means avalanche of electron and ion production that other neutral atoms are ionized due to collisions of secondary electrons in equation 2.1. The discharge is continued but the number of electrons in this range is still insufficient.

The plasma resistance is decreased with increasing current (increasing ions and electrons) at normal glow discharge of glow discharge. Therefore, The voltage is decreased and plasma is stabled. At this range, the number of ion production is equal to it of extinction. Also bright light is emitted at cathode (or target). The sputtering is processed in range of abnormal glow discharge that voltage is increased as function of current.

A arc discharge is induced with higher current and low voltages. It is consisted of non-thermal and thermal arc.
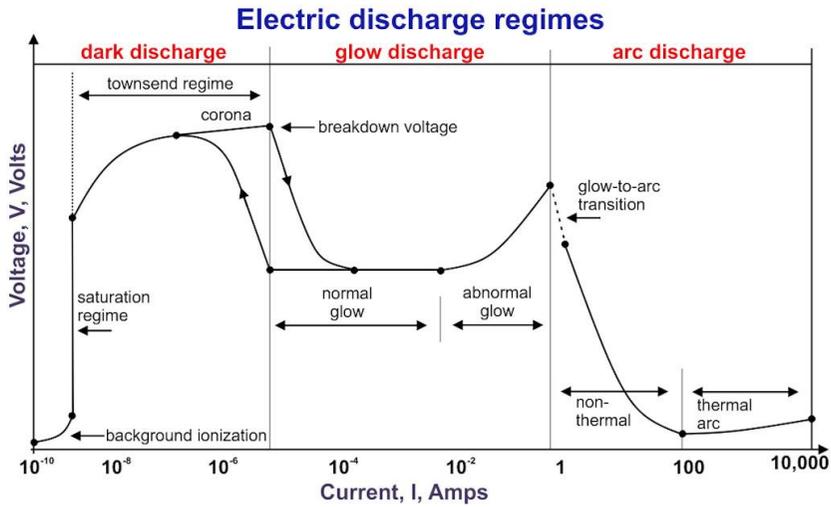
Figure 2.2 V-I graph of DC discharge [1]

2.1.2 Sputtering yield

A sputtering yield is defined as the number of atoms per colliding ion on the target. It is approximately calculated as below equation 2.2 at ion energies from 100 to 1000eV [2].

$$S = \frac{3\alpha}{4\pi^2} \frac{4m_i m_t}{(m_i + m_t)^2} \frac{E}{U} \ [atom/ion] \tag{2.2}$$

Where α is ratio of the masses of the target atom and the incident ion, m_i is the atomic mass of the bombarding incident ion, m_t is atomic mass of the target, E is energy of the incident ion, U is binding energy of the surface atom of the target. The sputtering yield is related to target material, gas, power according to equation 1.4.

Al target using inert gas of Ar is experimentally reported as value from 0.11 to 1.24 at different energies from 100 to 600eV [3].

2.1.3 Magnetron sputter

In order to increase the ionization rate of the target, a magnetron is provided on the cathode (target) side of the plate shaped diode so that the electrons stay in the electric and magnetic fields around the target, and the ionization is continued, so that sputtering is intensively caused and ionization is caused. There is an effect that the growth rate of the treated material is greatly increased. Also The swirling motion of the electrons can reduce the collision of the electrons with the substrate and the thin film. Therefore, the effect of increasing the substrate temperature is small.

2.1.4 Reactive gas sputter

Ar gas is usually used for sputtering due to cost and efficiency. However, the reactive gas sputtering for compound film growth is used as method supplying a small amount of oxygen or nitrogen besides Ar gas. Compound thin film formation by reactive gas sputtering is advantageous in terms of manufacturing, purity and cost, rather than direct sputtering of oxide or nitride targets. The reason is that sputtered atoms from target are in a very unstable state, so that they easily react with the reactive gas and the atoms that reach the substrate are also fast in the thin film state. Also sputtering yield of metallic target is over 100 times higher than it of compound target. Growth rate using metallic target is faster than using compound target. However, arc discharge is occurred in sputtering process [4,5]. Because reactive gas is affected as increasing compound fraction of metallic target.

2.1.5 Pulsed sputtering deposition (PSD)

The reactive gas sputtering has disadvantage of instable process called poisoned effect. The metallic target becomes poisoned insulator (nitride or oxide) with higher reactive gas. It functions as capacitance caused arching

in sputtering process. [4,5] PSD is presented as solution of this problems [5]. Reverse voltage is added at PSD compared with DC mode as shown in figure 2.3. At the reverse voltage ranges, electron and ions of plasma decay the dielectric surface. off voltage time (τ_{off}) is required for stable sputtering of on voltage time (τ_{off}). The relationship called duty cycle is defined as below equation 2.3 [6].

$$Duty\,cycle = \frac{\tau_{on}}{\tau_{on} + \tau_{off}} = \frac{\tau_{on}}{\tau_{cycle}} \qquad (2.3)$$

The arc free condition is related to the duty cycle and figure 2.4 shows their relationship. If not $\tau_{off.crit} > \tau_{off.crit}$ and $\tau_{on} < \tau_{on.crit}$, arc discharge is induced due to charging accumulation and dielectric surfaces. It is normally processed from 0.5 to 0.9 for relaxation of arc discharge.

Also Sputtering using pulsed supply was reported merit of high kinetic energy atoms supply. [7] It means possible that high energy migration length of ad atoms is supplied.
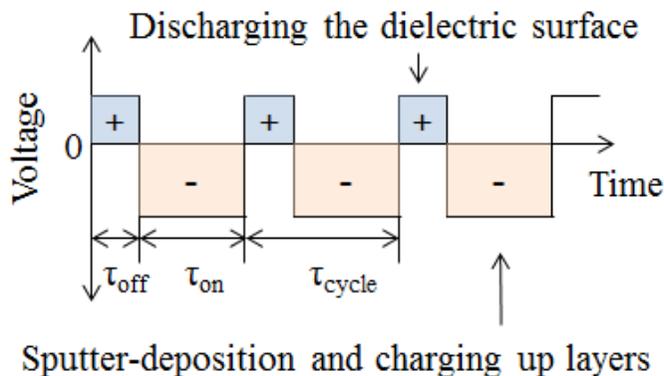
Figure 2.3 V-I graph of pulsed unipolar DC discharge
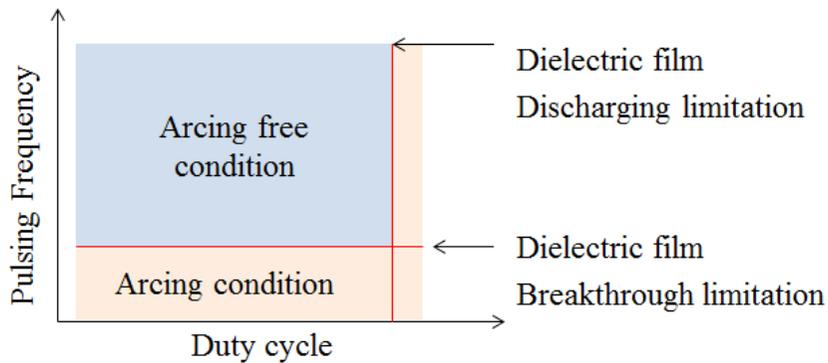
Figure 2.4 Arcing free conditions in the 2-d space of pulsing frequency and duty cycle

2.2 X-ray diffraction (XRD)

X-ray diffraction of each crystal lattice appears in the crystal, which is an important means for understanding the crystal structure. Figure 2.5 shows mechanism of X-ray diffraction. Due to shorter wavelength of X-ray (few Å) than lattice constant, X-ray can be passed between atoms and affected to tens of micrometer atoms. incident X-ray is reflected by each of the atoms and it disappears and the reflected wave does not exist. However, reflected X-ray does not disappear because the constructive interference occurs only when conditions satisfies Bragg's law as shown equation 2.1.

$$2dsin\theta = n\lambda \qquad (2.1)$$

Where d is plane distance, θ is diffraction angle, n is positive integer and λ is wavelength of X-rays (this research use Cu-Kα of 1.54184Å). The equation 2.1 means if sample has a constant d value (good alignment with c-axis) strong diffraction is happened only at a specific angle of incidence.

The XRD using this mechanism is analysis equipments of crystallinity by controlling XRD goniometer. Films are typically analyzed using XRD such as mismatch, phase, strain, preferred orientation, crystallite size relaxation, in-plane epitaxy, mosaic spread, thickness density

XRD is divided of parallel beam (PB) mode and Bragg Brentano (BB) mode as x-ray alignment. Figure 2.6 shows x-ray different modes. Focusing geometry beams is utilized in BB mode and parallel beams is utilized in PB mode. In this study, AlN thin films is investigated using theta-2theta scan of BB mode and using omega rocking curve, theta-2theta and phi scan in PB mode.
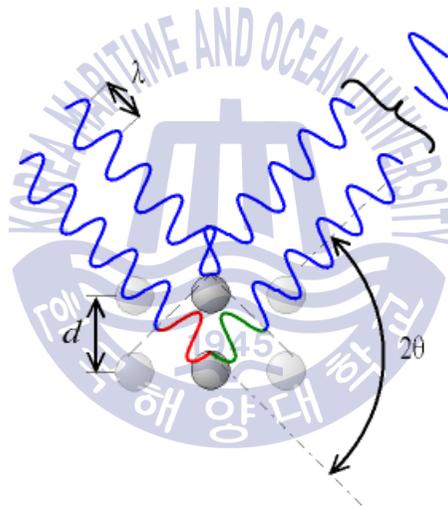
Figure 2.5 Bragg's law [8]
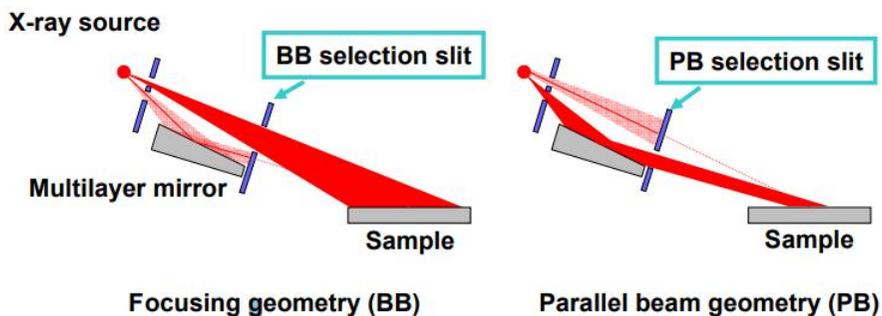
Figure 2.6 The schematic of BB and PB modes [9]

2.3 Atomic force microscope (AFM)

AFM, one of scanning probe microscope can analyze surface. Figure 2.7 shows configuration and mechanism of AFM. It is typically consisted of mirror, laser, cantilever, detecter. when probe of a few atoms size near approaching to sample, vibration is occurred because of van der waals force between probe and surface atoms. It is imaged using measured detector. The AFM has 2 measurement modes such as non contact mode and contact mode. They utilize applications of attractive and repulsive force of van der Waals force shown in figure 2.8 respectively. The non contact mode reduces damage to sample. However, resolution is lower than contact mode.

It has resolution of a few nanometer window. Therefore, films of narrow range is usually used for roughness, grain size and morphology.

In this study, It is used for roughness and morphology utilizing non contact modes for reducing damage to films. The size of 10×10 μm is observed in this study.
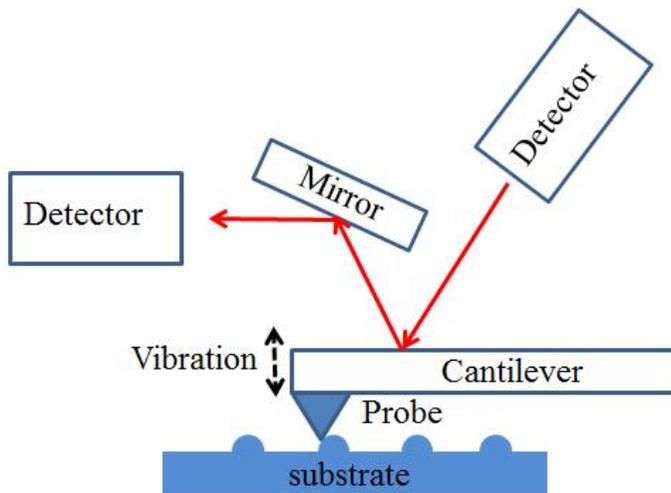
Figure 2.7 The schematic of AFM mechanism
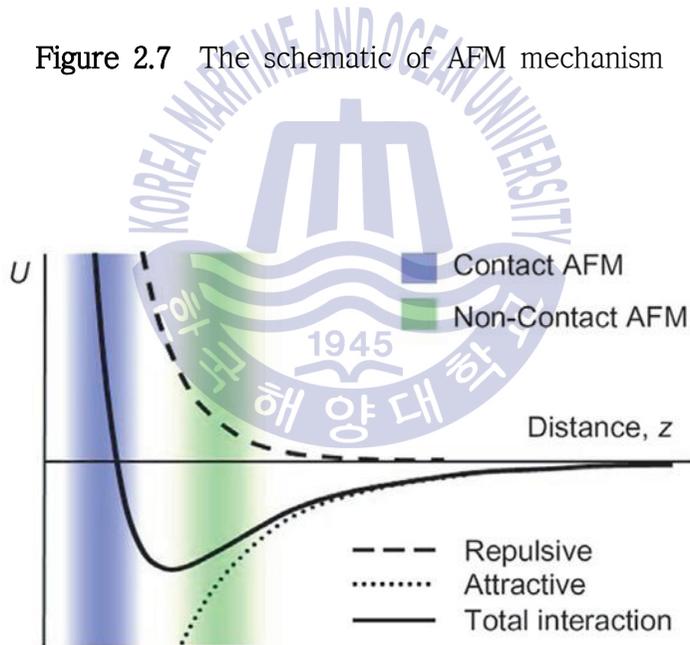
Figure 2.8 Different AFM modes using van der waals force [10]

2.4 Field emission scanning electron microscope (FE-SEM)

FE-SEM is a widely used microscope for observation of small size microstructure and shape in solid state. It forms surface images by using information of secondary electron generated as shown figure 2.8. Field emission using a tunneling effect, one of the methods for forming electrons can emit electrons at low temperature and high efficiency compared with a thermo electron emission.

FE-SEM has high spatial resolution of 0.8 – 1.8 nm. Also since it is a measurement method using electrons, there is a limitation that a sample is a conductor. In the case of a insulator or a semiconductor, a thin conductor layer must be coated for measurement.

In this study, thin carbon layer is coated on AlN layer reducing charging before measurement. It is used for surface morphology of AlN thin films at electron voltage of 15 kV.
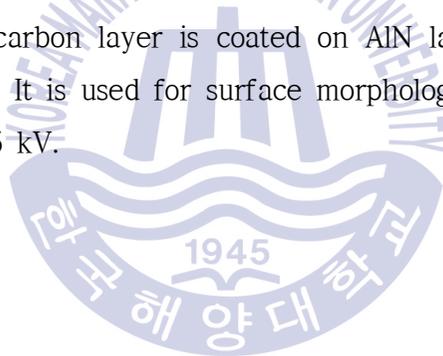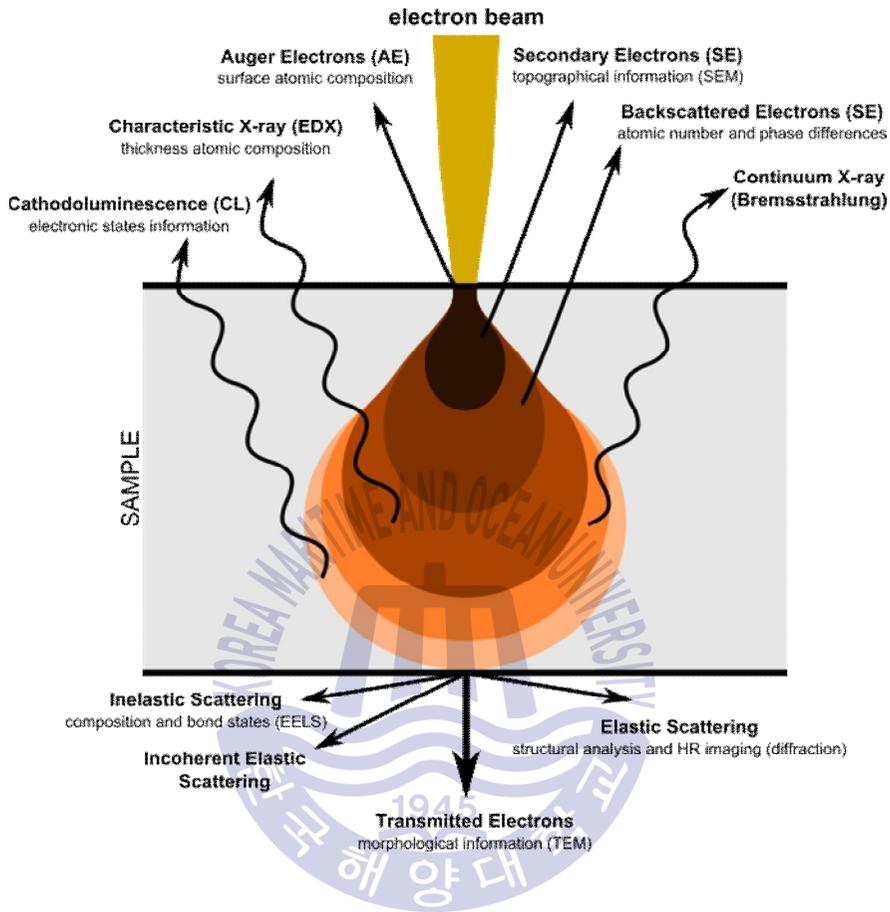
Figure 2.9 Different types of electron interactions with specimen and related detection modes [11]

2.5 Energy dispersive x-ray spectrometer (EDS)

EDS analyzes the components of a specimen using a characteristic X-ray of various signals, in which a high-energy electron beam reacts with the specimen as shown figure 2.9 and holds the structure and chemical composition information of the specimen.

EDS is capable of qualitative and quantitative analysis of materials. In qualitative analysis, X-rays of K-, L- and M-groups are distinguished. Since the peak position of the spectrum has an error of about 10 eV, it is possible to easily find the elements. However, when the peaks are closer to the resolution (128 eV), the peaks overlap. In this case, the electron acceleration voltage can be adjusted to enable accurate analysis. In case of quantitative analysis, it is analyzed through the peaks in qualitative analysis. It is calculated as atomic percent and weight percent by the algorithm of the system (ZAF). However, a peak resolution and accuracy in quantitative analysis is low, but it is very easy to use because it is very easy to use for beginners and it can process large amount of data due to its short signal acquisition time.

In this study, It is used for relative composition variation of AlN thin films as function of sputtering conditions.

2.6 Cathodoluminescence (CL)

The CL analyzes the components of a specimen using a electron state information as shown figure 2.9. Using an electron beam, electrons of the valance band are excreted, and it emits energy of a specific wavelength band is measured. The CL is variously applied to evaluation of impurities or defects such as semiconductors, evaluation of stress distribution, evaluation

of light emitting devices, and evaluation of three-dimensional quantum structure.

When electrons and holes meet and recombine in the semiconductor, they emit light or heat. The recombinations are divided as non-luminescent and luminescent recombination. Typical examples of non-luminescent recombination are defects, which include externally added impurity atoms, native defects, dislocations, and defect complexes, and inherent defects in compound semiconductors are intrusive an interstitial atom, a vacancy, and an antisite defect. However, some defects can also recombine with uminescent recombination. All these defects have energy levels different from those of the lattice-filled atoms and usually form one or several energy levels in the forbidden zone of a semiconductor. The energy levels in the forbidden zone effectively recombine the transporters, especially when the position of the energy level is near the middle of the forbidden band.

In this study, it is used for luminesce property of AlN such as defect and direct band gap.

2.7 Fourier transform infrared (FTIR)

FTIR is a measurement that can quickly measure all the materials in the state by absorbing infrared or transmit infrared rays by applying infrared rays to the sample.

When IR light enters to the substrate, the molecules that make up the material are subjected to specific vibrations depending on its structure. The energy of this molecular vibration becomes equal to the infrared light energy. For this reason, when infrared light is irradiated on a substance, only the light in a specific wave number area corresponding to the frequency of the vibration mode is absorbed. It is also effective in

qualitative and quantitative analysis, and quantitative analysis of organic substances in various mixtures can be carried out without a pre-treatment.

In this study, it is used for Al-N cluster of thin films. It is used to correlate Al-N cluster with sputtering conditions.

Reference

[1] User: Iantresman, 2011. *Wikipedia; electric glow discharge* [Online] (Updapted 6 March 2011) Available at: https://www.plasma-universe.com/File:Glow_D.jpg [22 October 2017]

[2] Andreeta, M. R. B., 2012. *Crystallization: science and technology.* InTech:Rijeka, Croatia.

[3] Laegreid, N., & Wehner, G. K., 1961. Sputtering Yields of Metals for Ar^+ and Ne^+ Ions with Energies from 50 to 600 ev. *Journal of Applied Physics,* 32(3), pp.365-369.

[4] Carter D.C., Arent R.L., & Chistie D.J., 2007. Sputter Process Enhancement through Pulsed-dc power. *Proceeding of the 50th Annual Technical Conference,* society of vacuum coaters:digital library

[5] Cater, D.C, 2008. Arc Prevention in Magnetron Sputtering Processes. *Proceedings of the 51st Annual Technical Conference,* Chicago, April 19-24, 2008, 2008 society of vacuum coaters:digital library

[6] Belkind, A. et al. 2000. Pulsed-DC reactive sputtering of dielectrics: pulsing parameter effects. *Proceedings of the 43rd Annual Technical Conference,* Denver, April 15-20, 2000, Vacuum coaters:digital library

[7] Stuart R. V., Wehner G. K., & Anderson G. S., 1969. Energy Distribution of Atoms Sputtered from Polycrystalline Metals. *Journal of Applied Physics*, 40, pp.803-812.

[8] Soukup R. J., Kulkarni A. K., & Mosher D. M., 1979. Electrical properties of sputtered epitaxial films of GaAs. *Journal of Vacuum Science and Technology*, 16 pp.208-211.

[8] User: Cdang, 2011. *Wikipedia; bragg' s law* [Online] (Updated 8 March 2011) Available at:

https://commons.wikimedia.org/wiki/File:Loi_de_bragg.png?uselang=ko [29 October 2017]

[9] Michael Bates, 2016. Xrd nanomaterials course_s2015_bates [Online] (Updated 12 April 2016) Available at: https://www.slideshare.net/MichaelBates30/xrd-nanomaterials-courses2015bates [17 December 2017]

[10] Park systems. 2017. *Basic Contact AFM & Dynamic Force Microscope (DFM)* [Online] Available at: http://www.parkafm.co.kr [29 October 2017]

[11] User: Claudionico~commonswiki, 2013. *Wikipedia; Scanning electron microscope* [Online] (Updated 17 December 2013) Available at: https://commons.wikimedia.org/wiki/File:Loi_de_bragg.png?uselang=ko [29 October 2017]

Chapter 3. Reactive Gas DC Magnetron Sputtering of AlN Thin Films

3.1 Introduction

In general sputtering, fundamental sputtering parameters such as plasma power and gas flow rate are relatively simple compared with other thin film growth methods. Although the substrate temperature can be varied, the general sputter growth usually proceed at room temperature. In the case of sputtering using a reactive gas as in this study, the sputtering process is changed by the reaction of the target surface. A sputtered total number of metal atoms (R) in the reactive gas sputtering process is given by equation 3.1 as follows [1].
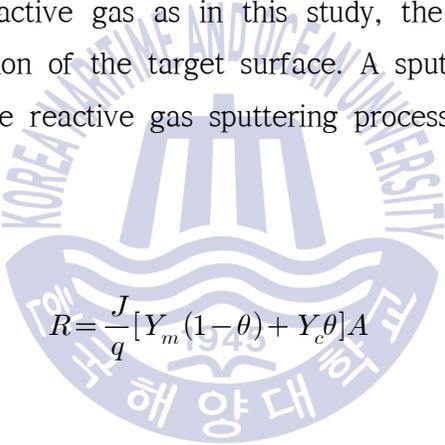
$$R = \frac{J}{q}[Y_m(1-\theta) + Y_c\theta]A \qquad (3.1)$$

Where J is the ion current density, q is the charge amount, Y_m is the sputtering yield of the target, θ is the surface area ratio of the target reacted with the reactive gas, Y_c is the sputtering yield of the compound formed by reacting with the reactive gas. Y_C has commonly higher value Y_m over 100 times. The equation 3.1 means sputtering parameter is relative to R value. In PVD mechanism, adhesion coefficient is close to 1 at room temperature. Therefore, the influence of the supply amount on the thin film is very large.

In this chapter, AlN films controlled as basic parameter of reactive gas DC sputtering is investigated as basic experiment for high quality AlN thin

film. Through the change of the growth rate, it is confirmed that the composition of the thin film is changed. In addition, the effect on the crystallinity was explained in terms of stoichiometric composition change.

3.2 Experimental details

Before growth, ITO (200 nm)/ SiO$_2$ (200 μm) substrates of 20×50mm size were cleaned as acetone, methanol and DI water during 10min respectively. AlN films were deposited on it using reactive gas DC magnetron sputter. In order to deposit AlN, N$_2$ gas of 6N and Al metal target of 5N were used at sputter. The basic sputtering parameters such as gas flow ratio (Ar flow of 10sccm and N$_2$ gas flow from 3 to 7 sccm) and plasma power from 75 to 300W were controlled at RT.

The analyses of surface were performed using FE-SEM and AFM. The $10\times10\,\mu$m^2 range were measured in AFM measurements. A films color variation was evaluated by photo camera. Crystallinity was evaluated using XRD. The X-ray source of Cu-kα is used for the XRD theta/2theta measurement. A relative composition of N and Al in the thin film is measured by EDS.

3.3 Influence of plasma power on reactive gas DC magnetron sputtering of AlN thin films

3.3.1 Growth rate variation

the growth rate increased linearly with increasing plasma power as shown figure 3.1. It was changed from 100nm/h of 75W to 750nm/h of 300W. It can be described by modifying equation 3.1 to equation 3.2 because of $Y_m\gg$

Y_c.

$$R = \frac{J}{q} Y_m (1-\theta) A \tag{3.2}$$

The plasma power is well known as plasma power = I×V. The current (I) affects to the ion current density as below equation 3.3 and the voltage (V) affects the sputtering yield as below equation 2.2 given at previous chapter.

$$J = \frac{I}{1+\gamma} \tag{3.3}$$

$$S = \frac{3\alpha}{4\pi^2} \frac{4m_i m_t}{(m_i + m_t)^2} \frac{E}{U} \quad [atom/ion] \tag{2.2}$$

where γ is secondary electron emission coefficient of a few percentage. The equation 3.2 is changed as below equation 3.4.

$$R = \frac{3\alpha}{4\pi^2} \frac{4m_i m_t}{(m_i + m_t)^2} \frac{1}{U} \frac{1}{1+\gamma} (1-\theta) A \times P \tag{3.4}$$

$$\approx K(1-\theta)P$$

where K is abbreviated constant. The equation 3.4 implies that the supply of Al is proportional to the plasma power. It is affected to films of increasing growth rate. Therefore, in figure 3.1, the increase in growth rate as increasing plasma power can be expected to be due to the increase in Al.
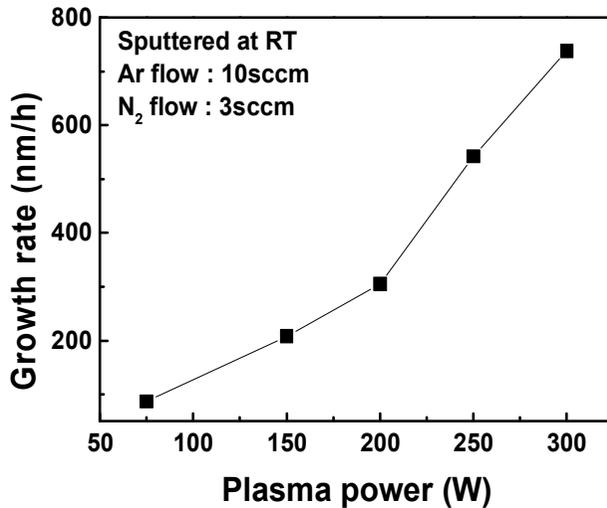
Figure 3.1 Growth rate of films with plasma power from 75 to 300W at N_2/Ar flow ratio of 3/10

3.3.2 Surface change

The plasma power is affected to Al supply amount. It is also expected that this phenomenon controls composition of film due to the amount of Al generated from the target.

Figure 3.2 shows surface of AlN thin films grown at different plasma power. The thin films in the plasma power range from 75 to 300W is described as photograph, top image of FE-SEM and roughness RMS value of AFM. AlN has a wide band gap and transmits to visible range. Therefore, high transparency is generally obtained. Transparent thin films were observed in the samples grown on plasma power (P<200W) (figure 3.2 (a) and (b)). A dark surface at high plasma power (P>200W) (figure 3.2 (c) (e)) were observed. Although the AFM Roughness RMS value of the same specimen shows a smooth surface at plasma power of 200W or less,

surfaces with a very rough and high density island structure were observed at a plasma power of 200W or more.

It is judged to be a droplet due to Al through a phenomenon appearing under high Al supply condition. Metallic droplet is similarly reported in AlN growth using MBE. [2] S. Tamariz et al. have reported that Al droplet is induced at high Al supply amount or low N supply amount condition. A 200W sample with a dark surface and no droplet is observed. It have been reported as a phenomenon appearing in an approximate region of stoichiometric composition called Al-rich intermediate region. [3] Also in the case of a wide band gap compound, the change in the transparency of the sample observed with the naked eye is most likely caused by a change in the stoichiometric composition. In the case of AlN, if the composition is changed, metallic Al in the thin film is formed and transparency is reduced.

the amount of Al supplied increases with the increase of the plasma power, and it is expected that the change of the stoichiometric ratio causes the change of the transparency and the surface roughness.

(a) P=75W
RMS=0.7nm
Gr=87nm/h

(b) P=150W
RMS=1.2nm
Gr=208nm/h

(b) P=200W
RMS=1.3nm
Gr=305nm/h

(d) P=250W
RMS=37.0nm
Gr=542nm/h

(e) P=300W
RMS=93.0nm
Gr=738nm/h
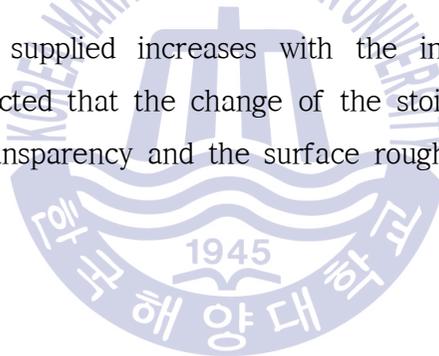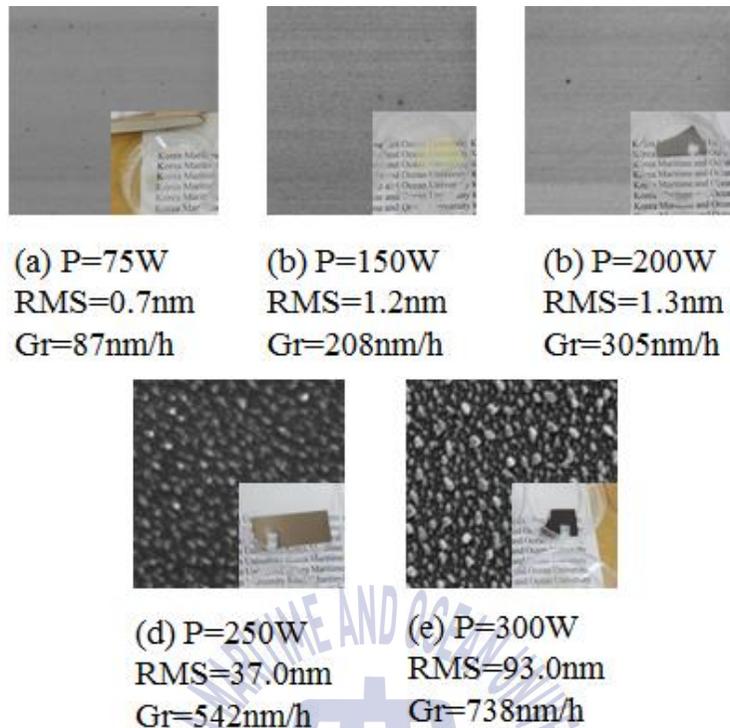
Figure 3.2 Surface of AlN samples grown at different plasma power

3.3.3 Composition variation

It was expected that the stoichiometric composition is changed as increasing plasma power in previous chapters. EDS results were confirmed to intuitively confirm the stoichiometric composition change of the thin film as shown figure 3.3.

As a result of the intensity change of N and Al peaks according to the change of plasma power, N/Al ratio of films was decreased linearly as increasing plasma power. Ⅴ/Ⅲ > 1 at low power and Ⅴ/Ⅲ < 1 at plasma power of 200W or more were observed. Also from results, it is expected that a stoichiometric condition is obtained at plasma power of about 180W in this experiment.

The films of low N/Al ratio have been reported to induce Al droplets in AlN growth using MBE. [3] In this experiment, similar results at Al rich condition (250 and 300W samples) is observed. 200W As a result, it is confirmed that the plasma power influences the stoichiometric composition of the thin film by increasing the Al supply.
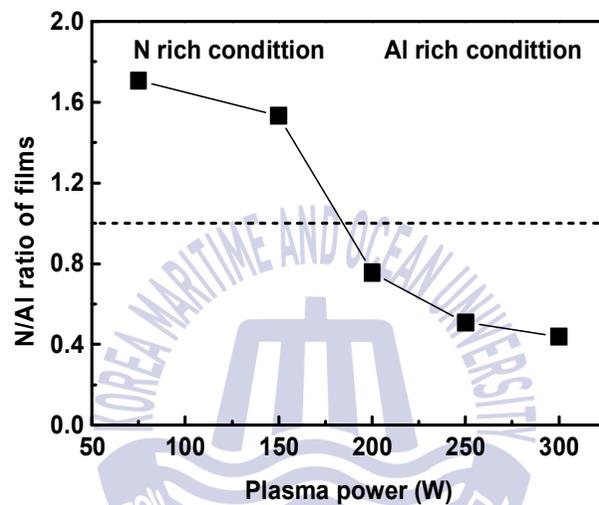
Figure 3.3 Relative composition at different plasma power

3.3.4 Crystallinity

The XRD $2\theta-\theta$ patterns were observed for describing the effect of stoichiometric composition on crystallinity. Figure 3.4 shows XRD $2\theta-\theta$ pattern at plasma power from 75 to 300W the ITO and SiO_2 related peaks did not show any change in position or intensity in all samples. On the other hand, the AlN (0002) peaks were hardly observed at low plasma power conditions (<150 W), However the highest intensity was observed at 200 W and the tendency was rather decreased when the power is higher. Also, metallic Al (111) peaks were observed, which are clearly

distinguishable from samples grown at high plasma power of 250W and 300W. and the intensities of the peak were increased with an increase in the plasma power, it can be judged that the supply amount of Al is increased with an increase in the plasma power. Considering that the nitrogen gas supply was fixed in this experiment, the reason why the diffraction intensity of AlN at a power of 200W shows the greatest strength is that this condition is interpreted as the most suitable condition for AlN growth from the stoichiometric viewpoint.
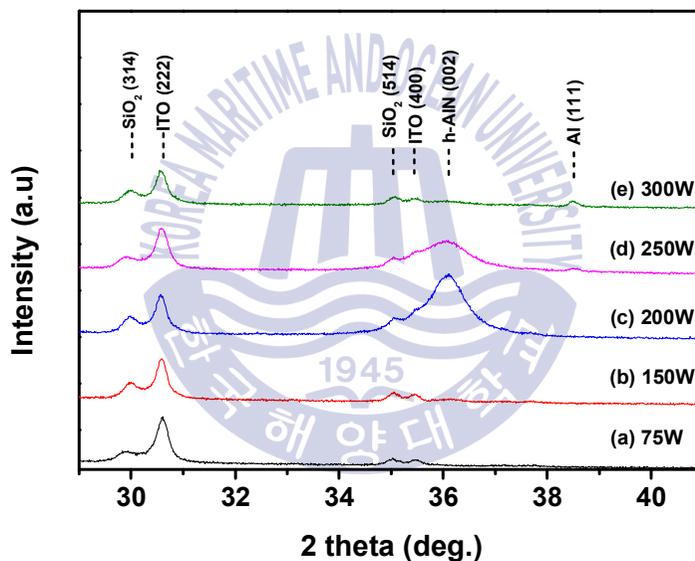
Figure 3.4 XRD theta-2theta patterns of sputtered AlN layers on ITO/SiO$_2$ at different plasma power

To sum up the results so far, through the change of the growth rate, it can observe that the amount of Al was controlled by plasma power. Also the composition of the thin film was changed due to it. Figure 3.4 (a) and (b) can be classified as those in which the supply amount of N is higher

than that of Al. It is referred to as the so called N-rich condition. In the N-rich condition, the thin film showed a smooth surface and transparency in the visible region. In figure 3.4 (c) – (e), the range was growth condition of Al oversupply. In the Al-rich condition, the thin film showed dark color and a rough surface because of Al droplet. These conditions affected the crystallinity. It was also confirmed that the proper amount of Al is important for the crystallinity of the thin film.

3.4 Influence of gas flow ratio on reactive gas DC magnetron sputtering of AlN thin films

In the sputtering process, the reactive gas is known to be consumed in three ways as below [1]

(1) Move to a vacuum pump
(2) React with the target to form a compound
(3) Activated in the plasma and supplied to the substrate

As the reactive gas supply increases and the nitrogen partial pressure in the growth chamber increases, the ratio of reacting with the target surface also increases. If this phenomenon persists, it may prevent stable plasma generation in extreme cases. Therefore, even if the supply amount of the reactive gas is controlled, the range in which the plasma stability is ensured is checked in advance, It is important to control the gas flow rate in the condition.

At higher N_2 gas flow than 7 sccm, it interfered with formation of high density plasma. Therefore, the flow rate of nitrogen was limited to 7 sccm or less. In this experiment, Ar gas flow rate was fixed to 10 sccm and N_2

gas is injected from 3 to 7 sccm. The effect of gas flow ratio on the thin film was confirmed by the change of growth rate and the effect on the crystallinity from the viewpoint of stoichiometric composition.

3.4.1 Growth rate variation

Figure 3.5 is the result of the change of growth rate according to the variation of nitrogen flow rate at various plasma power. The growth rates at every plasma power conditions were decreased with increasing the nitrogen flow rate.

In the experiment in which the plasma power was fixed, the tendency of the growth rate to decrease with the increase of the nitrogen flow rate is not explained at (1) phenomenon of gas flow ratio. For example, if the growth rate is determined by the supply amount of the growth element, the growth rate of the thin film increases as the supply amount of nitrogen increases while the plasma power is constant (constant amount of Al supply). Therefore, it can be seen that the decrease in growth rate in figure 3.4 should be explained as (2) phenomenon rather than (1) phenomenon. Therefore, it can be described by the poison fraction of target (θ) in equation 3.4.

$$R \approx K(1-\theta)P \qquad\qquad (3.4)$$

where K is abbreviated constant, θ is fraction of poisoned target, P is plasma power. Through the above equation, as the nitrogen flow increases, θ value increases, and the supply amount decreases, and as a result, the growth rate decreases.
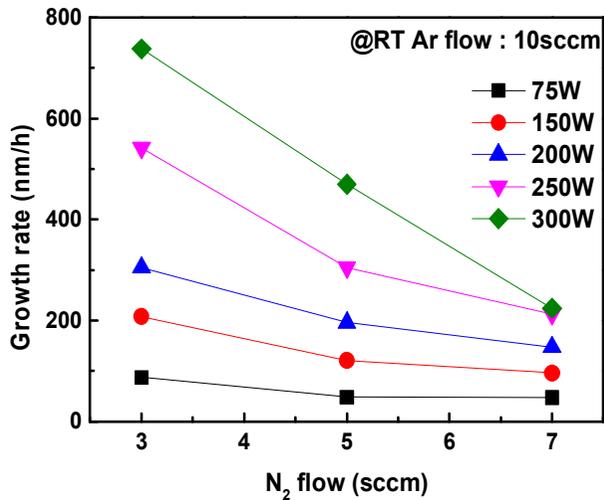
Figure 3.5 Growth rate according to the variation of nitrogen flow
rate at various plasma power from 75 to 300W

3.4.2 Surface variation

The cause of figure 3.5 was explained by surface analysis in figure 3.6.
Figure 3.6 is surface variation at conditions of different N_2 gas flow. In the
results of figure 3.2, the change of the transparency and the surface
roughness of the sample were observed at conditions of different plasma
power. Figure 3.6 (a) was observed as similar the metallic surface, but
figure 3.6 (b) of 5 sccm and figure 3.6 (c) of 7 sccm increased
transparency. Also, the sample grown at 3sccm was described island like
structures originating from the metal phase in the AFM images, and those
grown at 5 and 7sccm were observed flat surfaces without island like
structures.

The results can be actually concluded that Al supply is decreased by
increasing the nitrogen flow rate (2) phenomenon. In the gas flow ratio
control, the smooth surface is observed because of the increased N and
decreased Al supply.
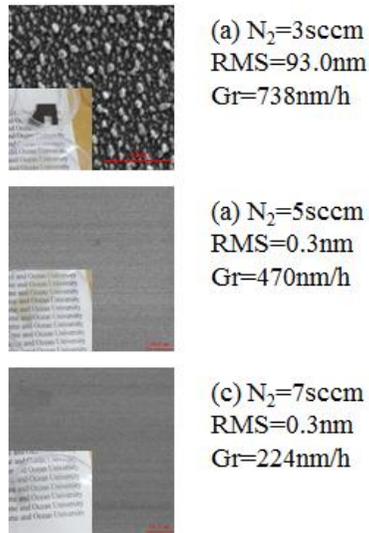
Figure 3.6 FE–SEM image, photo image, AFM roughness RMS value and growth rate of the grown AlN samples as function of N_2 gas flow

3.4.3 Crystallinity and relative composition variation

Figure 3.7 shows investigation of composition and crystal quality of the sample grown according to the above mentioned change. Figure 3.7 (a) show the XRD intensity changes of AlN (002) and Al (111). It have been reported that the preferred orientation change of AlN was observed depending on the mixing ratio of the reactive gas [4]. However, in the experiment, thin films of all conditions were observed as the c–axis orientation. As the nitrogen flow rate increased, the Al peak intensity decreased and the intensity of AlN peak increased with XRD. The decrease of the Al peak intensity and the increase of the AlN peak intensity were considered to be due to the increase of the N supply amount and decrease of Al supply amount with the increase of the nitrogen flow rate.

Figure 3.7 (b) is the intensity ratio of N and Al peaks measured by EDS at this condition. The Ⅴ/Ⅲ ratio of the thin film measured by EDS was

increased with increasing the nitrogen flow rate. As expected, it can be interpreted as a result indicating that as increasing supply amount of N, the reactive gas has reacted on the target surface and the sputtering yield of the target has decreased to reduce the Al supply amount. As a result, the sample grown at gas flow of 7sccm is close to the superior stoichiometric composition (near 1 of Ⅴ/Ⅲ ratio).
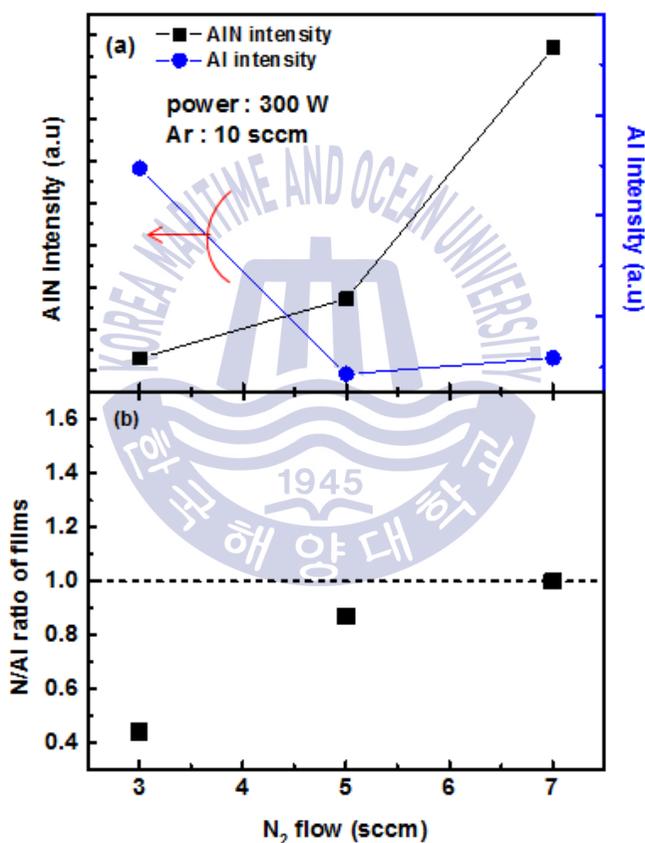
Figure 3.7 (a) The XRD theta-2theta intensity of AlN and Al peaks and (b) The chemical ratios variation of AlN thin films as function of N₂ gas flow

3.5 Conclusion

In chapter 3, AlN thin films on the ITO/SiO$_2$ substrate were investigated by reactive gas DC magnetron sputter. The plasma power and gas flow ratio (increasing N$_2$ gas flow) at reactive gas DC sputter were controlled. The growth rates varied with sputtering parameters, confirming that the Al supply amount was controlled. The influence of the thin film was analyzed in terms of stoichiometric composition according to the change of the Al supply amount. The stoichiometric composition influenced the crystallinity of the film. As result, it is considered for high quality AlN fabrication process.

Reference

[1] Depla, D., & Mahieu, S., 2008. *Reactive Sputter Deposition.* Springer:Berlin, Heidelberg.

[2] Tamariz S., Martin D., & Grandjean N. 2017. AlN grown on Si(111) by ammonia-molecular beam epitaxy in the 900–1200 $^{\circ}$C temperature range. *Journal of Crystal Growth*, 476, pp.58-63.

[3] Pan J.-H. et al., 2011. Epitaxy of an Al-Droplet-Free AlN Layer with Step Flow Features by Molecular Beam Epitaxy, *Chinese Physics Letter*, 28, 068102

[4] Iqbal, A., Walker, G., Iacopi, A., & Mohd-Yasin, F., 2016. Controlled sputtering of AlN (002) and (101) crystal orientations on epitaxial 3C-SiC-on-Si (100) substrate. *Journal of Crystal Growth*, 440, pp.76-80.
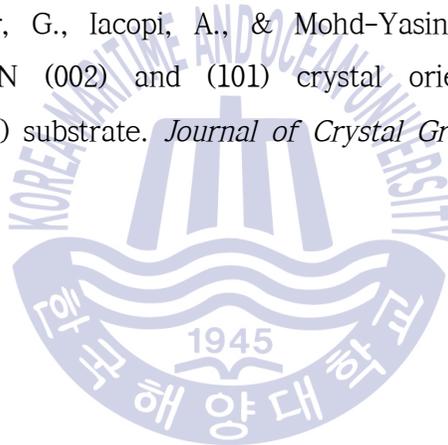
Chapter 4. Pulsed Sputtering Deposition of AlN Thin Films

4.1 Introduction

The improved crystallinity of AlN thin films is essential for a wide range of applications. Pulsed power supplies in the PLD method can supply high energy Ⅲ-group precursors, which can reduce defect density at low growth temperatures. [1] The PSD method, which the positive voltage supplies in addition to the DC power supply, is a similar growth method to PLD in that it uses a pulsed power supply. K. Sato et al. reported the possibility of fabricating high quality AlN thin films on SiC with low lattice mismatch with AlN using PSD. [1]

There are many parameters in the sputtering method, and as the sputter of this chapter uses pulsed DC, the parameters that control the waveform of the voltage such as pulsed frequency and off time are additionally introduced in comparison with DC. PSD is similar to reactive gas DC magnetron sputter but it is reported that residual strain is formed in thin film due to high energy of Al supply. [2] To fabricate high quality AlN thin films, using sputter it is necessary to study it and it can be improved by using parameters in PSD. [3-5]

In this chapter, the sputtering conditions of PSD are optimized for high quality AlN. In previous chapters, sputtering parameters affected the Al supply and altered the stoichiometric composition of the film. It also affected the crystallinity. Using it, chapter 4 investigated the effect of sputtering parameters on the thin film and the solution of the problem in terms of lattice strain variation of the thin film.

4.2 Experimental details

AlN thin films were deposited on a 2 inch double side polished (DSP) – sapphire wafer using PSD. Before the growth, the substrates were cleaned by ultrasonic cleaning for 10 minutes each for acetone, methanol, and DI-water for organic cleaning. Sputtering parameters such as gas pressure from 0.1 to 1.2 mtorr, Ar gas flow from 10 to 15 sccm, N_2 gas flow from 7 to 10 sccm, substrate growth temperature from room temperature to 500 $^{\circ}$C and a plasma power from 300 to 800 W were controlled. Pulsed DC pulse frequency of 50 kHz and off time of 2.0 μs (Duty cycle: 0.9) were confirmed in arc free condition.

Sputtered AlN thin films under various conditions were fabricated with similar thicknesses of 700 $\pm$ 30 nm for comparison. The grown AlN thin film analysis is analyzed by growth rate, thin film color, relative composition and crystallinity. The growth rate was measured using a contact profiler, and the color change of the film was observed using a photo camera. The composition change of the thin film was measured by EDS at 5 kV electron beam condition, and EDS intensity was converted into atomic precent and compared with N/Al intensity ratio values. Al-N clusters are analyzed using FTIR at wavenumber of 500 to 1800 cm^{-1}. Crystallinity was evaluated using XRD and Cu-kα was used as an X-ray source. The measurements used theta-2theta scan, omega rocking curve scan and phi scan. The omega rocking curve scan is controlled as the omega value at theta-2theta peak position (36.04°) of bulk AlN (0002). The phi scan was measured at the chi angle of 42.729 degrees, which is the angle between AlN (0002) and AlN (10-12), and theta-2theta angle of AlN (10-12), which is 49.821 degrees. The lattice strain of the thin film was calculated as shown in equation 4.1 below.

$$\sigma_c = \frac{c_{film} - c_{bulk}}{c_{bulk}} \tag{4.1}$$

Where c_{film} is the c-axis lattice constant of the thin film, c_{bulk} is c-axis lattice constant of bulk AlN (AlN = 4.982 Å). c_{film} calculated the peak position of XRD theta-2theta using Bragg's law of equation 2.1.

4.3 Influence of plasma power on the PSD AlN thin films

Plasma power of the reactive gas DC magnetron sputter in chapter 3 affected the Al supply. As a result, the composition of the thin film was changed and it affected the crystallinity. However, the plasma power in PSD was mainly have been reported as a parameter to increase the migration length during AlN growth. [3] However, Al atoms of high energy induce residual strain, which is expected to affect the crystal quality of the thin film. [2] In addition, high plasma power in PSD is expected to affect crystallinity as Al supply also increases. In this chapter, the effect of plasma power on the film. is investigated.

4.3.1 Al amount supply

Figure 4.1 shows the growth rate of AlN thin films grown at various plasma powers from 300 to 800W. Other sputtering parameters such as the pulsed frequency of 50 kHz, the off time of 2.0 μm, the Ar/N_2 gas flow ratio of 3/2 and room temperature are fixed. As the plasma power increases, the growth rate increases linearly from 220 to 1439 nm/h.

Figure 4.2 shows the color of these films. Samples with low power conditions are transparent in visible light, but as the plasma power increases, the film gradually darkens. It is similar to the results of using

reactive gas DC magnetron sputtering in chapter 3. Therefore, plasma power is also influenced by Al supply in PSD.

Figure 4.3 shows the change in the N/Al EDS intensity ratio. As the plasma power increases, the N/Al EDS intensity ratio decreased linearly from 1.2 to 0.75. It can confirm the effect of the thin film on the increased Al supply. As the Al supply increased, the N/Al EDS intensity decreased, and the Al supply also affected the composition.

Consequently, the results show that the plasma power in the PSD also affects the Al supply, which influences the composition of the film.
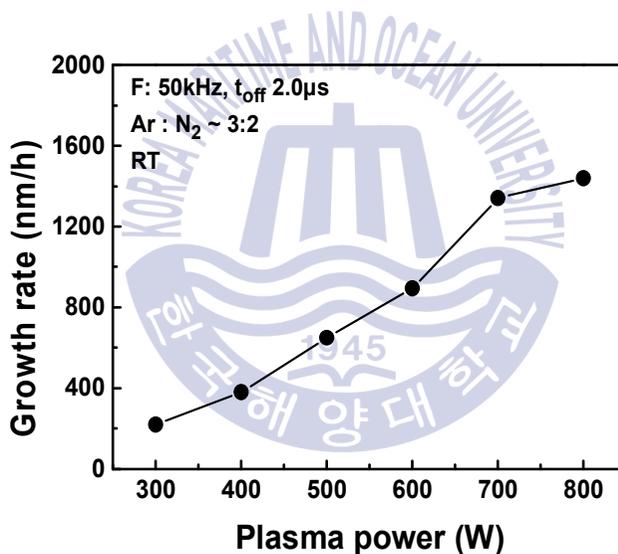
Figure 4.1 Growth rate at different plasma power from 300 to 800W
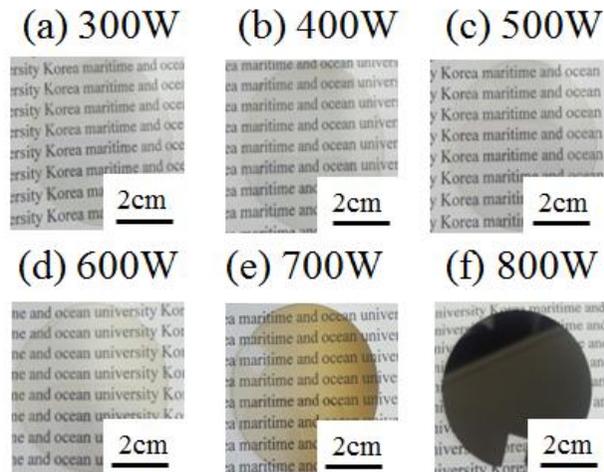
Figure 4.2 Films color at different plasma power from 300 to 800W
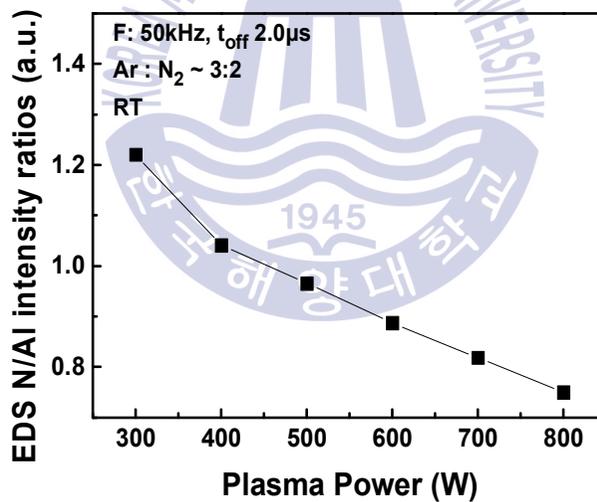
Figure 4.3 EDS N/Al intensity ratio at different plasma power from 300 to 800W

4.3.2 Migration length

The results in chapter 4.3.1 were very similar to the results of DC (chapter 3). However, PSD can supply molecules of higher energy rather than DC sputter. [6,7] The high energy Al atoms increase AlN crystallinity due to migration length increase. [3]

Figure 4.4 shows the change in thin-film peaks FWHM of theta-2theta patterns. In conditions of plasma powers from the 300 to 600W, the FWHM decreases linearly as the plasma power increases. However, FWHM increased sharply from 600 to 800W.

In the regions of low plasma power, the plasma power is increased and the crystallinity of the thin film was increased by increasing the energy of Al molecules. However, in the regions of high plasma power, as the plasma power increases, the crystallinity was expected to deteriorate due to the plasma damage.
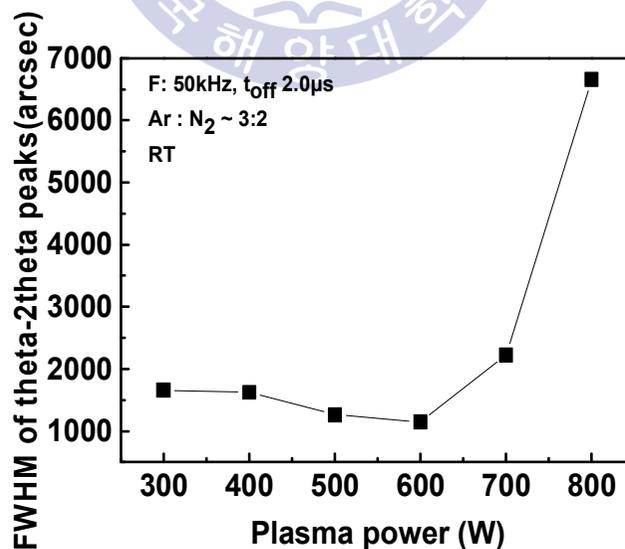
Figure 4.4 FWHM of theta-2theta peaks at different plasma power from 300 to 800W

4.3.3 Plasma damage

Plasma damage can be identified in the XRD theta-2theta patterns in shown figure 4.5. The peak positions of the grown thin film were shifted from the bulk h-AlN peak position (36.04°) to a lower angle from 0.14 to 0.26° as the plasma power increased. It indicates that the thin film has a tensile strain in the c-axis direction, and the plasma power has a lattice strain relationship. Similar results [2-5] were observed in the AlN thin films grown with PSD, which are reported to be caused by the peening effect. Thornton and Hoffman have reported when metal molecules of high-energy are deposited on a substrate, the molecules collide with the substrate and induce a residual strain. [2] When high-energy metal atoms are supplied, compressive strain appears when the tensile strain is supplied with low-energy atoms.

Al peaks due to Al supply were not observed in XRD patterns. Samples in the high plasma power (600-800 W) range were similarly observed in chapter 3, although the color of the thin film was observed to be dark, but the Al peaks were not confirmed. These conditions are considered to be the effects of the Al-rich intermediate condition. [8]
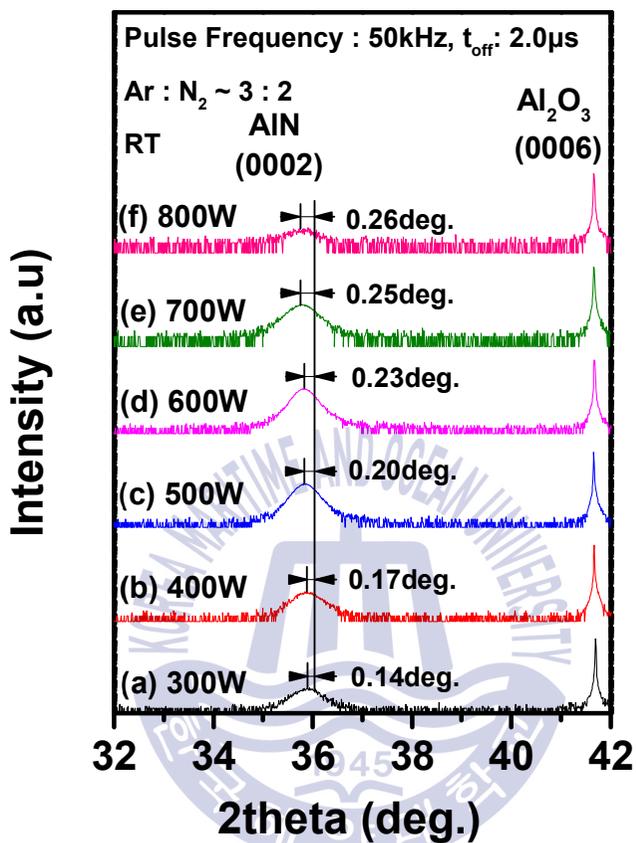
Figure 4.5 Theta-2theta patterns at different plasma power from 300 to 800W

4.3.4 Lattice constant

In XRD patterns, the films had tensile strain in the c-axis direction. Figure 4.6 shows their c-axis lattice constant of samples. The lowest lattice constant of 300W (4.996 Å) was higher than bulk AlN (4.979 Å), and the lattice constant increased linearly from 4.996 to 5.013 Å as the plasma power increases.

It means that thin films has a residual strain, and The tendency increases with increasing plasma power. Therefore it is concluded that plasma power generates plasma damages.
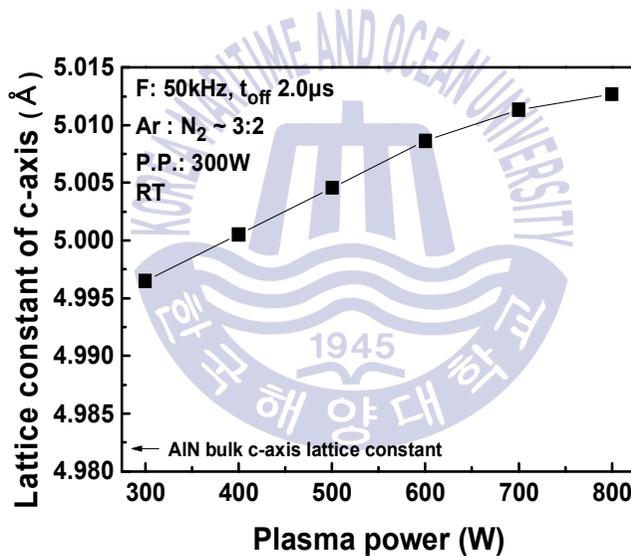
Figure 4.6 Lattice constant of films at different plasma power from 300 to 800W

4.3.5 Al-N cluster

High-energy Al penetrated into the thin film, resulting in defects due to residual strain. Strain due to peening was expected to be induced in Al-N clusters. Al-N clusters have various geometric arrangements as shown in Figure 4.7. Table 4.1 shows the theoretical calculation results. [9]

Table. 4.1 Reported geometries of Al-N clusters used in the theoretical calculation [9]

| Cluster	Distance	Geometry	Wavenumber	IR	Raman
Al$_2$N	Al−N=1.731	$^2\Sigma_n^+$	133.3 cm^{-1}	23.67	0
			525.4 cm^{-1}	0	11.13
			1052.4 cm^{-1}	86.14	0
Al$_3$N$_2$	Al−N=1.705 N−Al=1.713	$^2\Sigma_u^+$	42.4 cm^{-1}	6.97	0
			154.0 cm^{-1}	29.53	0
			376.4 cm^{-1}	0	83.17
			675.9 cm^{-1}	201.19	0
			1166.3 cm^{-1}	1098	0
			1167.3 cm^{-1}	0	166.68
AlN$_2$	Al−N = 1.804	$^1\Pi_u$	157.2 cm^{-1}	53.9	0
			163.9 cm^{-1}	81.1	0
			646.2 cm^{-1}	0	706
			660.1 cm^{-1}	1036	0
AlNNN	Al−N = 1.826 N−N = 1.206 N−N = 1.138	$^1\Sigma^+$	97.1 cm^{-1}	0.85	7.38
			496.4 cm^{-1}	141	42.3
			627.0 cm^{-1}	21.2	0.89
			627.8 cm^{-1}	21.2	0.89
			1463.3 cm^{-1}	277.8	0.26
			2266.9 cm^{-1}	850	48.7
AlN$_2$Al	Al−N = 1.888 N−N = 1.204	$^3\Sigma_g^+$	73.2 cm^{-1}	4.4	0.2
			209.6 cm^{-1}	0.1	19.26
			332 cm^{-1}	8.7	676
			606 cm^{-1}	341.6	10.67
			1744 cm^{-1}	7.9	5878
Al$_3$N	Al−N = 1.850	D_{3h}	156.3 cm^{-1}	3.8	5.1
			223.62 cm^{-1}	0.2	0
			427.52 cm^{-1}	0	56.9
			749.44 cm^{-1}	326.4	0.10
			749.46 cm^{-1}	326.4	0.11

Figure 4.8 shows the FTIR spectra results to confirm the effect of high residual strain. Al-N clusters of Al_2N ($521cm^{-1}$), AlN_2Al ($591cm^{-1}$), AlN (620-$670cm^{-1}$) and Al_2N_3 ($1339cm^{-1}$) were observed in all samples. It expect that residual strain was associated with Al-N clusters.

Therefore, it is necessary to confirm the correlation between plasma power and Al-N cluster. Figure 4.9 shows the variation of Al-N cluster intensity with plasma power. The intensities of Al_2N and Al_2N_3 clusters increased linearly with increasing plasma power. In other words, Al-N cluster interacts with the peening effect.

From these results, it can be seen that the AlN thin film needs to be fabricated at low plasma power in order to reduce the residual strain. However, low plasma power also reduces migration length. The crystal quality is judged to be lower and further studies on other sputtering conditions are needed.
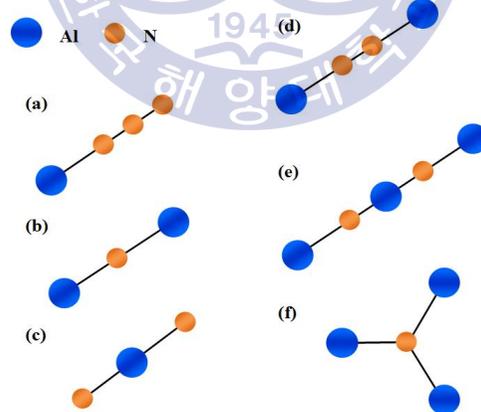

Figure 4.7 Geometric arrangement of clusters of Al_xN_y such as (a) AlNNN, (b) Al_2N, (c) AlN_2, (d) Al_2N_2, (e) Al_3N_2 and (f) Al_3N
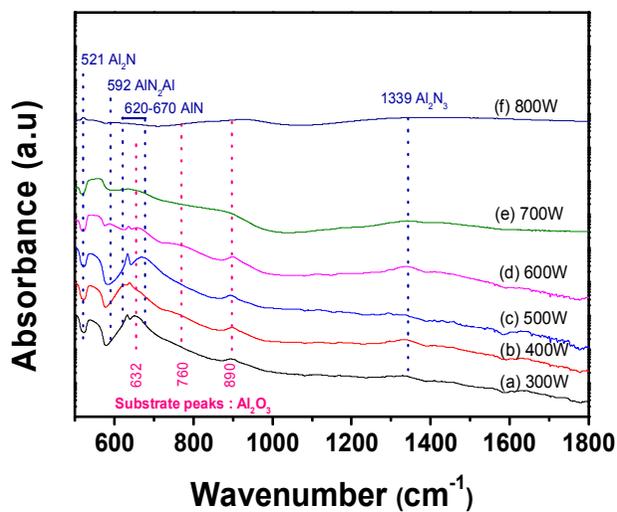
Figure 4.8 FTIR spectra at different plasma power from 300 to 800W
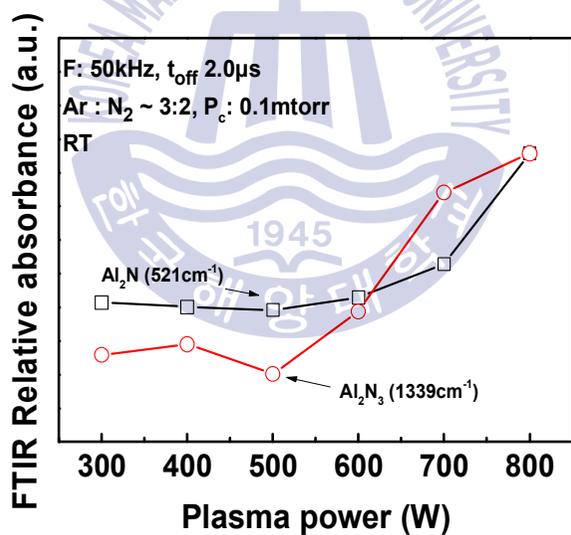
Figure 4.9 FTIR relative absorbance at different plasma power from 300 to 800W

4.4. Influence of gas pressure on the pulsed sputtering deposition of AlN thin films

The gas pressure of sputtering conditions is commonly used as an element to increase the aspect ratio. The lower pressure can be supplied as highly directional sputtered molecules of a high aspect ratio to the thin film. Also the gas pressure is related to a mean free path of the atoms and have been reported as a sputtering parameter that can control the residual strain. [4] M. Ohtsuka et al. has reported the effect of gas pressure on AlN thin films that high gas pressure at low mean free path can reduce residual strain due to peening effect. [4]

In this experiment, too low (<0.1 mtorr) high (> 1.2 mtorr) pressure was plasma unstable. Therefore, It was investigated at stable plasma forming conditions of 0.1 to 1 mtorr.

Figure 4.10 shows the change in residual strain at gas pressures in the range of 0.1 to 1 mtorr. As the gas pressure increased, the residual strain decreased from 0.002 to 0.008. It has been demonstrated as the Al atoms of energy decreased due to reduced mean free path. [4]

Figure 4.11 shows the variation in FWHM at gas pressures ranging from 0.1 to 1 mtorr. As the gas pressure increased, the FWHM increased from 0.57 to 0.58. The reason for the deterioration of the crystallinity is that the migration length is expected to decrease as the energy of Al atoms decreases due to the reduced mean free path.
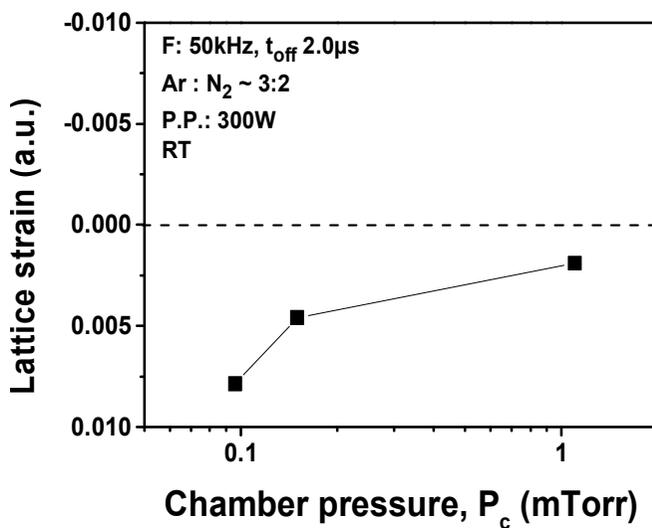
Figure 4.10   Lattice strain at different chamber pressure from 0.1 to 1 mtorr
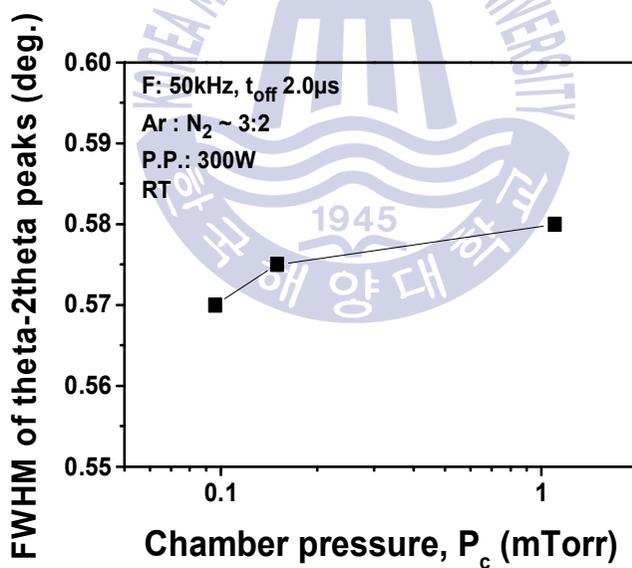

Figure 4.11   FWHM of theta-2theta peaks at different chamber pressure from 0.1 to 1 mtorr

4.5 Influence of substrate growth temperature on the pulsed sputtering deposition of AlN thin films

Previously, the gas pressure decreased the residual strain, but decreased the crystallinity. The parameters related to the Al supply energy generated during sputtering were limited in that the crystal quality and the residual strain were inversely proportional to each other. Therefore, the anode parameters such as the substrate growth temperature influenced after the Al supply need to be adjusted. In previous studies, the substrate growth temperature was reported to increase the surface migration length. [10]

Figure 4.12 shows the change in theta-2theta peak FWHM of AlN thin films prepared from room temperature to 500 ℃. As the growth temperature increases, the FWHM of the thin film is decreased from 0.57 to 0.28 deg due to the increase of the surface movement length.

Figure 4.13 shows the lattice strain from room temperature to 500 ℃. The lattice strain also was decreased with increasing temperature. At 500 ℃, thin films with the same lattice constant were observed compared to bulk AlN. Al-N clustering is also expected to decrease.

The substrate growth temperature in the PSD affected to increase both the crystal quality and the lattice strain due to the increase of the surface movement length.

Figure 4.14 shows the XRD patterns of films grown at room temperature, 300 ℃ and 500 ℃. The high FHWM and residual strain were observed at room temperature, and FHWM and residual strain decrease with increasing temperature.

Figure 4.15 shows these phi-scan patterns. In the samples at RT and 300 ℃, no peaks were observed due to low crystallinity and high strain results. It can expect the presence of large amounts of tilt and twist dislocation. However, in a sample at 500 ℃, a 6-fold symmetric peaks at 60° intervals

were observed, which means that the wurtzite structure of AlN is well aligned. In addition, improvement of crystallinity of in plane can be judged to have a high c-axis direction because defects such as dislocation are reduced. Table 4.2 summarizes the results measured by various methods of XRD.

Table. 4.2 The values of various XRD measurements at different growth temperature

	ω rocking curve FWHM	θ−2θpeak FWHM	φ scan
HT−AlN (500℃)	1.53 deg.	0.28 deg.	6−fold
LT−AlN (300℃)	3.01 deg.	0.34 deg.	U.A.
RT−AlN (30℃)	8.61 deg.	0.58 deg.	U.A.

As a result, a thin film approximating to residual strain of 0 was fabricated at a growth temperature of 500 ℃, an Ar / N_2 gas flow ratio of 3/2, and a plasma power of 300 W. The crystallinity with 6-fold symmetry was observed (ω rocking curve FWHM: 1.5 deg. θ-2θ peak FWHM: 0.28 deg.).
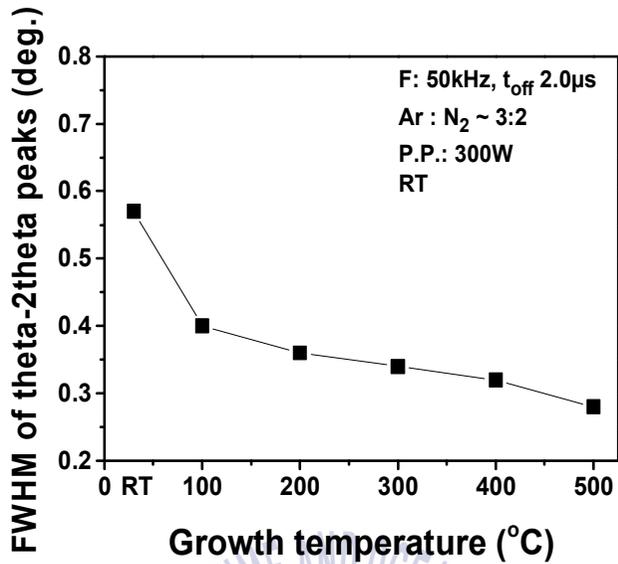
Figure 4.12 FWHM of theta-2theta peaks at different growth temperature from RT to 500℃
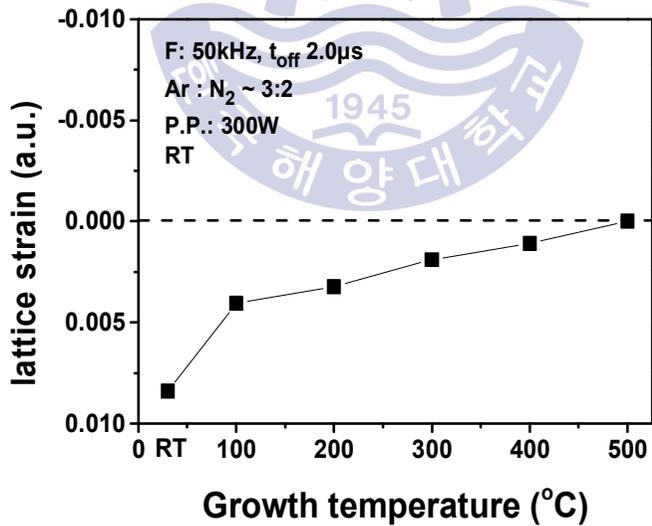
Figure 4.13 Lattice strain at different growth temperature from RT to 500℃
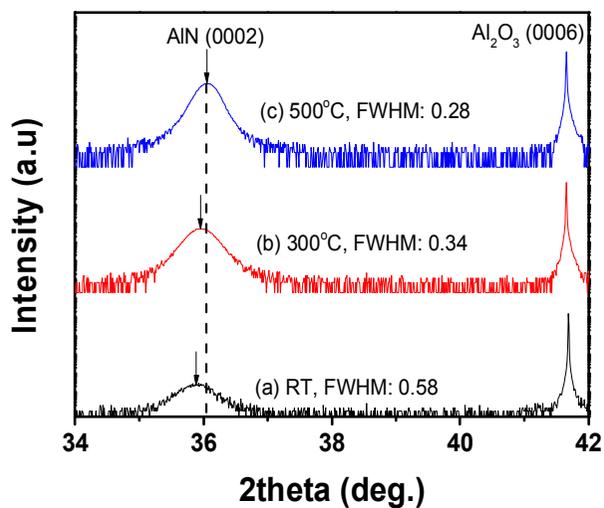
Figure 4.14 XRD theta-2theta patterns of (a) RT, (b) 300 ℃ and (c) 500 ℃
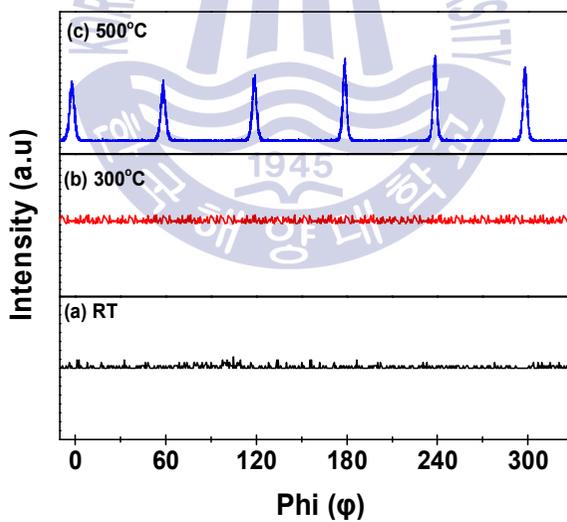
Figure 4.15 XRD phi patterns of (a) RT, (b) 300 ℃ and (c) 500 ℃

4.6 Conclusion

In this chapter, the PSD condition of the AlN thin film was optimized.

Plasma power affected the amount of Al and the chemical stoichiometry of the film as well as migration length and plasma damage. Plasma damage induced residual strain, which was directly related to Al-N cluster.

The gas pressure was able to reduce the residual strain in relation to the mean free path of Al molecules, but the high gas pressure was induced to poor crystallinity due to low energy Al atoms.

As the growth temperature increased, both crystallinity and residual strain were improved.

Using these a thin film approximating to residual strain of 0 was fabricated at a growth temperature of 500℃, an Ar/N$_2$ gas flow ratio of 3/2, and a plasma power of 300W. The crystallinity with 6-fold symmetry was observed.
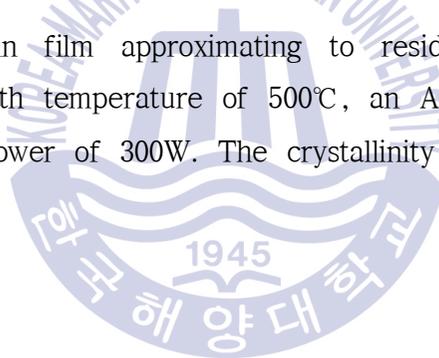
Reference

[1] Sato, K. et al., 2009. Room-Temperature Epitaxial Growth of High Quality AlN on SiC by Pulsed Sputtering Deposition. *Applied Physics Express*, 2(1), 011003.

[2] Thornton, J. A. & Hoffman, D. W., 1977. Internal stresses in titanium, nickel, molybdenum, and tantalum films deposited by cylindrical magnetron sputtering. *Journal of Vacuum Science and Technology*, 14(1), pp.164-168.

[3] Takeuchi, H., Ohtsuka, M., & Fukuyama H., 2015. Effect of sputtering power on surfacecharacteristics and crystal quality of AlNfilms deposited by pulsed DC reactive sputtering. *Phys. Status Solidi B*, 252(5), pp.1163-1171.

[4] Ohtsuka, M., Takeuchi, H., & Fukuyama, H., 2016. Effect of sputtering pressure on crystalline quality and residual stress of AlN films deposited at 823 K on nitrided sapphire substrates by pulsed DC reactive sputtering. *Japan Society of Applied Physics*, 55, 05FD08.

[5] Cherng J. S., & Chang D. S., 2010. Effects of pulse parameters on the pulsed-DC reactive sputtering of AlN thin films. *Vacuum*, 84, pp.653-656.

[6] Stuart, R. V., Wehner, G. K., & Anderson, G. S., 1969. Energy Distribution of Atoms Sputtered from Polycrystalline Metals. *Journal of Applied Physics*, 40, pp.803-812.

[7] Soukup, R. J., Kulkarni, A. K., & Mosher, D. M., 1979. Electrical properties of sputtered epitaxial films of GaAs. *Journal of Vacuum Science and Technology*, 16 pp.208-211.

[8] Pan J.-H. et al., 2011. Epitaxy of an Al-Droplet-Free AlN Layer with Step Flow Features by Molecular Beam Epitaxy, *Chinese Physics Letter*, 28, 068102

[9] Correa, R. B., Rodríguez-García, M. E., & Mora, Á. P. 2014. Annealing effect on vibration modes of aluminum nitride thin films. *Mometnto-Revista de Física*, 48, pp.64-76.

[10] Barshilia, H. C., Deepthi, B., & Rajam K.S., 2008. Growth and characterization of aluminum nitride coatings prepared by pulsed-direct current reactive unbalanced magnetron sputtering. *Thin Solid Films*, 516, pp. 4168-4174.

Chapter 5. Characterizations of AlN Thin Films

5.1 Introduction

AlN has characterizations that can be used in various fields such as DUV-LED, RF filter, SAW sensor, heat sink, transparent device and memory device. However, AlN thin films fabricated by sputtering have advantages such as a higher possibility of a low temperature growth, a low roughness of thin film and a low manufacturing cost, but it is not satisfying in terms of crystallinity for certain applications. A study on the characterization of sputtered AlN thin films is needed for wide application of AlN. Therefore, It is important to evaluate feasibility of AlN thin film sputtered.

In this chapter, the characterizations of AlN thin films fabricated with PSD were studied and evaluated to determine the feasibility of various fields.

5.2 Experiment details

The surface, refractive index, luminescence characteristics, permittivity and resistance of the samples of LT-AlN (700 nm)/Al_2O_3 (XRC FWHM: 3.02 deg.) And HT-AlN (700 nm)/Al_2O_3 (XRC FWHM: 1.53 deg.) were evaluated. On the surface, the AFM was measured in the range of 10×10 μm^2. FE-SEM measurements were performed under accelerating voltage of 5 kV. and carbon coating was performed on the films before measurement. The refractive index (n) and extinction coefficient (k) were measured at wavelengths ranging from 300 to 1000 nm using an ellipsometer. The luminescence property was measured from 1.5 to 7 eV using CL at 80K.

The dielectric constant was measured in the region of 1 to 4000 MHz using VNA. I-V characterization was measured by fabricating Au/AlN/Al$_2$O$_3$ samples. Figure 5.1 shows a side view of the structure (a), and (b) OM top view image. Two upper Au metals were deposited on AlN/Al$_2$O$_3$ using a thermal evaporator. The thickness of Au is 100 nm and the distance between Au metals is 0.6 mm.
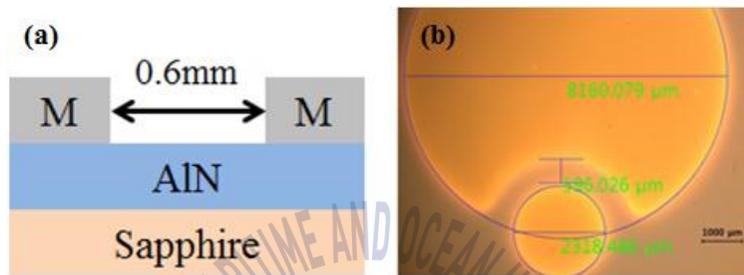
Figure 5.1 (a) The schematic and (b) OM top view image of fabricated MIM structure

5.3 Surface morphology

Figure 5.2 is the surface observed by various methods such as (a) photomicrograph and (b) FE-SEM (c) AFM 3D image of HT-AlN/Al$_2$O$_3$. In figure. 5.2 (a), the transparent characterization was observed in the visible light region and shows the value as a transparent device. The AlN material has a wide band gap and high transmittance in the visible region. In the case of sputtered AlN/glass, transmittance of over 83% was reported in the visible region. [1] In addition, a research has been reported about a transparent device, which is an ITO/AlN/ITO/glass structure. [2]

In figure 5.2 (b) and (c), a very smooth surface with a roughness RMS

value of less than 1 nm is observed. Sputtered AlN films were similar to previous results reported to have low roughness. [3,4] Roughness affects SAW characteristics. The smooth surfaces are required to minimize frequency variations due to local acoustic velocity changes. [5,6] Low roughness shows the research value as a SAW device.

Figure 5.2 (a) Photo image, (b) FE-SEM and (c) AFM 3D image of sputtered HT-AlN/Al$_2$O$_3$

5.4 Refraction index

Figure 5.3 shows a changes in refractive index (n) and extinction coefficient (k) of HT-AlN/Al$_2$O$_3$ depending on the wavelength range from 300 nm to 1000 nm. The value of n is 1.8, which is similar to the reported values of AlN/Glass (1.6) [3] and AlN/Si (1.9) [4].

Also, the value of k was approximated to 0 in the measured wavelength range. This is related to the absorption coefficient (β) as shown in equation 5.1, which means that light of a specific wavelength can be transmitted before it is absorbed.

$$\beta = \frac{4\pi k}{\lambda} \qquad (5.1)$$

In the case of semiconductors, absorption coefficient curves have sharp edges in light with energy below the band gap. It can be seen that k ≈ 0 in all wavelength regions and has a low absorption coefficient.
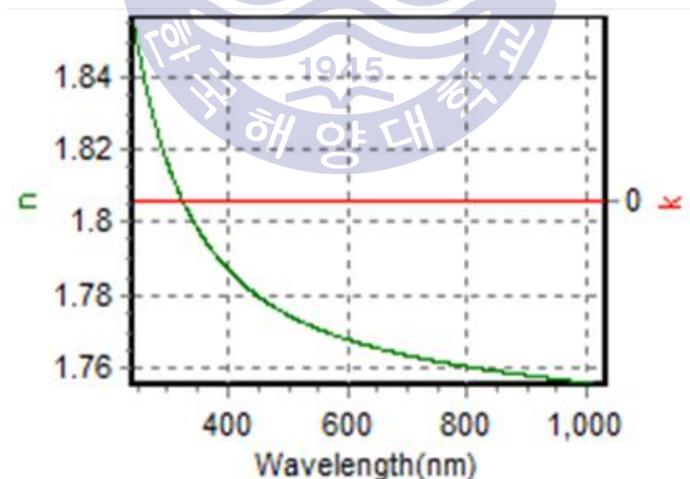
Figure 5.3 n and k value of sputtered HT-AlN/Al$_2$O$_3$

5.5 Luminescence property

Figure 5.6 shows CL spectra ranging from 1.5 to 7 eV at a low temperature of 80 K. Defects such as 3.00 eV nitrogen vacancy (V_N) and 4.67 eV interstitial (O_N) were observed in all samples of HT-AlN/Al_2O_3 and HT-AlN/Al_2O_3. [7] Near-band edge emission is also observed in LT-AlN/Al_2O_3.
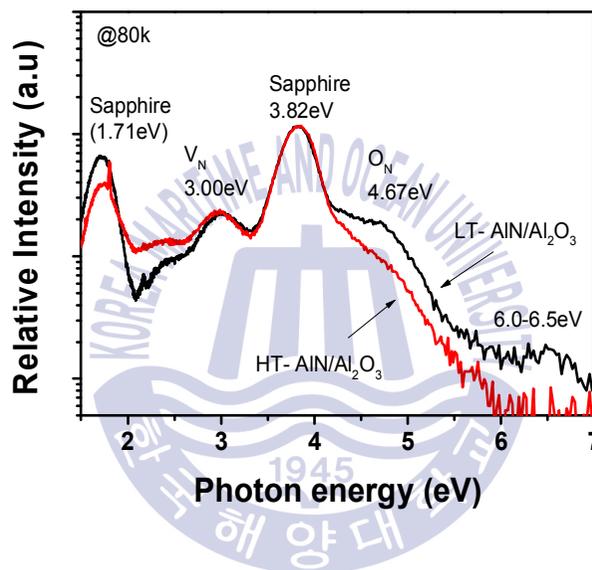
Figure 5.4 CL spectra of HT-AlN/Al_2O_3 and LT-AlN/Al_2O_3 at 80K

5.6 Relative permittivity

The dielectric properties can be determined by the memory device. The nitride material is characterized by low voltage/current capability. [8-10] Due to the thermal, dielectric and optical properties of AlN thin films, H. D. Kim et al. have been reported that AlN thin films have excellent value as transparent resistive random access memory (T-ReRAM) devices. [2]

Figure 5.4 shows the variation of dielectric constant according to the frequency of Al_2O_3 substrate, LT-AlN/Al_2O_3 and HT-AlN/Al_2O_3. Regardless of frequency, all samples is observed as parallel permittivity values. The relative dielectric constant of the AlN thin film at 1 MHz was

$$Al_2O_3 \ (4.6) < LT-AlN/Al_2O_3 \ (6.27) < HT-AlN/Al_2O_3 \ (6.5)$$

These values are similar to sputtered AlN films reported as values between 6.0 and 7.0. [4]
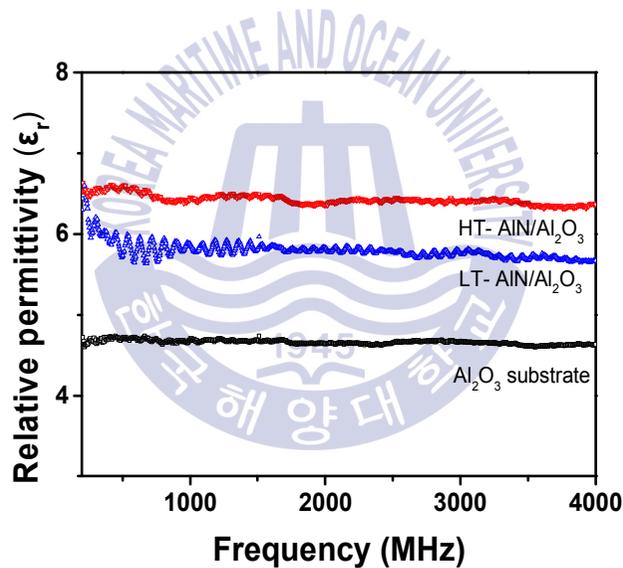
Figure 5.5 Relative permittivity of substrate, LT-AlN/Al_2O_3 and HT-AlN/Al_2O_3 as a function of test signal frequency

5.7 Electrical resistivity

Figure 5.8 shows the I-V curve from -5V to 5V for $Au/LT\text{-}AlN/Al_2O_3$ and $Au/HT\text{-}AlN/Al_2O_3$. Electrical resistivities (ρ) of $Au/LT\text{-}AlN/Al_2O_3$ (2.83×10^{11} Ωm) and $HT\text{-}AlN/Al_2O_3$. (4.24×10^{10} Ωm) were observed. These values are similar to the values for the resistive bulk AlN $\rho = 10^9 - 10^{11}$ Ωm. [11].
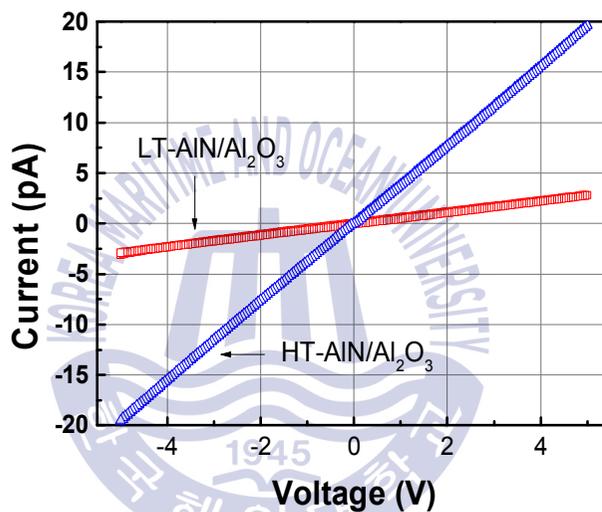
Figure 5.6 I-V curves of $LT\text{-}AlN/Al_2O_3$ and $HT\text{-}AlN/Al_2O_3$

5.8 Conclusion

In this chapter 5, evaluation of AlN thin films using PSD was investigated for feasibility. Table 5.1 shows properties of AlN thin films compared with AlN thin films on different substrates.

Table 5.1 The properties of reported AlN compared with this study

Property	AlN/Si	AlN/Glass	In this study, AlN/Al$_2$O$_3$
Surface	1nm	1.7nm	<1nm
Refraction index	1.9	1.6	1.8
Relative permittivity	–	6.0 ~ 7.0	5.7 ~ 6.5
Luminescence property	–	–	6.3 eV (Near band edge)
Electrical resistivity	–	$10^{10} \, \Omega\,m$	$10^{10} \sim 10^{11} \, \Omega\,m$

The surface of AlN thin films by PSD has low roughness, transparency at visible region. The value of refraction index and the relative permittivity were similar compared with previous research.

As a result, It has similar characteristics compared with the AlN thin films studied in the past, which indicate that research and development of devices using AlN thin films by PSD is possible.

Reference

[1] Dimitrova, V., Manova, D., & Valcheva, E., 1999. Optical and dielectric properties of dc magnetron sputtered AlN thin films correlated with deposition conditions. *Materials Science and Engineering*, B68, pp.1-4

[2] Kim, H.-D., An, H.-M., Seo, Y., & Kim, T. G., 2011. Transparent Resistive Switching Memory Using ITO/AlN/ITO Capacitors. *IEEE Electron Device Letters*, 32(8), pp.1125-1127.

[3] Kumari, N., Singh A. K., Barhai, & P. K., 2014. Study of Properties of AlN Thin Films Deposited by Reactive Magnetron Sputtering. *International Journal of Thin Films Science and Technology*, 3 pp.43-49

[4] Andrzej Stafiniak et al., 2009. Properties of AlN_x thin films prepared by DC reactive magnetron sputtering. Optica Applicata 39(4) pp.717-722

[5] Wang, D. Y., Nagahata, Y., Masuda, M., & Hayashi, Y., 1996. Effect of nonstoichiometry upon optical properties of radio frequency sputtered Al-N thin films formed at various sputtering pressures. *Journal of Vacuum Science and Technology A*, 14(6), pp.3092-3099

[6] Hsiosaki, T., Harada, K., & Kawabata, A., 1982. Low-Temperature Growth of Piezoelectric AlN Film and its Optical and Acoustical Properties. *Proceedings of Japan Journal of Applied Physics*, 21, pp. 69-71

[7] Slack, G. A., Schowalter, L. J., Morelli, D., & Freitas, J. A., 2002. Some effects of oxygen impurities on AlN and GaN. J*ournal of Crystal Growth*, 246(3-4), pp.287-298.

[8] Kim, H.-D., An, H.-M., Kim, K. C., Seo, Y., Nam, K.-H., Chung H.-B., Lee, E. B. & Kim, T. G. 2011. Improved reliability of Au/Si_3N_4/Ti resistive switching memory cells due to a hydrogen post-annealing treatment. *Journal of Applied Physics*, 109(1), pp. 016 105-1-016 105-3,

[9] Kim, H.-D., An, H.-M. & Kim, T. G., 2010. Large resistive-switching phenomena observed in Ag/Si$_3$N$_4$/Al memory cells. *Semiconductor Science and Technology*, 25(6), pp. 065 002–065 005.

[10] Chen, C., Yang, Y. C., Zeng, F., & Pan, F., 2010. Bipolar resistive switching in Cu/AlN/Pt nonvolatile memory device. *Applied Physics Letters*, 97(8), pp. 083 502-1–083 502-3.

[11] Kumari, N., Singh, A. K., & Barhai, P. K., 2014. Study of Properties of AlN Thin Films Deposited by Reactive Magnetron Sputtering. *International Journal of Thin Films Science and Technology,* 3(2), pp.43–49.

Chapter 6. Conclusion

In this study, growth and evaluation of AlN thin films were investigated for widen application of it. The AlN thin films have been deposited by sputter of two types such as DC mode and Pulsed DC mode. The characterization of AlN thin films using by PSD was investigated such as surface morphology, refraction index, relative permittivity, luminescence property and electrical resistivity.

Plasma power and N_2/Al gas flow ratio were controled as fundamental experiments using by reactive gas DC magnetron sputter. the sputtering parameters were affected to Al supply amount. It changed the stoichiometric composition of the film. In the N-rich condition, the thin film showed a smooth surface and transparency in the visible region. In the Al-rich condition, the thin film showed dark color and a rough surface because of Al droplet. These conditions affected the crystallinity. It was also confirmed that the proper amount of Al is important for the crystallinity of the thin film.

The sputtering parameters such as plasma power, gas pressure and substrate growth temperature were controled for optimization of AlN growth condition using by PSD. In PSD, also plasma power affected to Al supply amount. However, residual strain, such as tensile strain in the c-axis direction, was observed due to high energy Al supply during sputtering. Also It indicated that Al-N clustering has to be solved. The plasma power and gas pressure were correlated with the kinetic energy of Al supplied, and the relationship between crystal quality and lattice strain was inversely proportional to each other. The substrate growth temperature was controlled, and the crystal quality as well as the lattice strain were also decreased. Using these, a thin film without residual strain was fabricated with 6-fold symmetry.

Feasibility of AlN thin films using by PSD was investigated. It has similar characteristics compared with the AlN thin films studied in the past. It indicates that research and development of devices using sputtered AlN is possible.

Resume

1. Personal Data

Name	(Korean) 조성민 (English) Cho Sungmin (Chinese character) 趙成珉		
Ages/Sex	26 / Man	**Date of birth**	1991. 11. 18
E-mail	Sungmin1118@kmou.ac.kr		
Tel.	052)269-1258	**H.P.**	010-6471-1258
Address	#906, 14, Daegongwonipgu-ro, Nam-gu, Ulsan South Korean		

2. Education

Master of Engineering (Graduating in Feb. 2018)

Department of Convergence Study on the Ocean Science and Technology, Graduate School of Korea Maritime and Ocean University (KMOU)

Busan, Republic of korea

(Scholarship by KIOST and KMOU)

2016.03. ~ 2018.02.

Bachelor of Engineering (Graduated)

Major of Electronic Material Engineering, Korea Maritime and Ocean University

Busan, Republic of korea

2010.03. ~ 2016.02.

High school (Graduated)

Natural sciences, Ulsan Jeil Highschool

Ulsan, Republic of korea

2007.03. ~ 2010.02.

3. Experience

"China-Japan-Korea" Ocean Science, Technology Cooperation Education (Japan, TUMSAT), ERASUMS
Prof. Ohnuki Hitoshi, and Prof. Baba Ryo Lab.

2017.02.08. ~ 2017.02.11.

Selected best paper award, KIEEME Annual Autumn Conference 2016
Subject: Property of AlN Thin Film on ITO/SiO_2 Substrate by Reactive DC Magnetron Sputtering.

2016.11.18.

ICDL Start Certificate

2015.04.01.

Selected excellence award, 2014 Second half Capstone Design Contest
Subject: Buoy for coastal aquaculture damage prevention

2014.12.19.

Completed industrial field practice course, Korea Testing and Research Institute (KTR)
Composite material department

2014.06.23. ~ 07.18.

4. Participate in Research Project

Deep UV (200nm) surface emitting device by using AlN as a lighting emitting layer
Participating Researcher
- AlN thin films growth using sputter

2015.11 ~ until now

Development of HNS spill response information supporting technologies based on HNS dispersion model
Participating Researcher
- Fabrication of HNS detecting sensor based ITO powder

2016.01 ~ 12

5. Patent

Berth facility for preventing painting of new building ship from getting damaged (Patent application, Republic of korea)

patent application number: 10-2015-0046149

2015.04.01.

5. Research Paper

[1] **Cho, S.**, Choi, J., Choi, S., Cho, Y., Lee, S., & Chang, J., 2017. Investigation on the Growth of Tungsten Carbide Layer as a Buffer for GaN-on-Si Technology. *Journal of the Korean Institute of Electrical and Electronic Material Engineers*, 30(1), pp.1-6.

[2] **Cho, S.**, Lee, M., Lee, S., & Chang, J., 2017. Stoichiometric Composition Variation of the AlN Thin Films Grown by Using Reactive DC Magnetron Sputtering. New Physics: Sae Mulli, 67(8), pp.929-935.

[3] Koo, J., Lee. S., **Cho, S.**, & Chang, J., 2017. Effect of Additives on the Properties of Printed ITO Sensors. *Journal of Korean Physical Society*, 71(6), pp.335-339.

[4] Choi, J., Ko, D., **Cho, S.**, Lee, S., & Chang, J., A study on the crystallinity change by heat treatment of AlN thin films grown by pulsed sputter deposition *New Physics: Sae Mulli*, (accepted)

[5] **Cho, S.**, Choi, S., Cho, Y., Lee, S., Lee, M., & Chang, J., Molecular Beam Epitaxy Growth of GaN Films on Tungsten Carbide/Si Template. *Thin Solid films*, (submitted)

6. Presentation in the Conference

[1] **Cho, S.**, Cho, Y., Koo, J., & Chang, J., "Luminescence property of AlN based deep-UV light emitter device", KIEEME Annual Summer Conference 2016, Gyeongju, Republic of korea, June 2016.

[2] **Cho, S.**, Choi, S., & Chang, J., "MBE growth of single crystal GaN thin films on the Si substrate by using the Tungsten Carbide buffer layer", KIEEME Annual Summer Conference 2016, Gyeongju, Republic of korea, June 2016.

[3] **Cho, S.**, Choi, S., Cho, Y., Lee, S., & Chang, J., "The study of Si-GaN technology using Tungsten Carbide buffer layer", The 18th International Symoposium on the Physics of Semiconductors and Apllications, Jeju, Republic of korea, July, 2016.

[4] Koo, J., Lee. S., **Cho, S.**, & Chang, J., 2017. "Effect of Additives on the Properties of Printed ITO Layers", The 18th International Symoposium on the Physics of Semiconductors and Apllications, Jeju, Republic of korea, July, 2016.

[5] **Cho, S.**, Cho, Y., Kwon, H., Lee, M., & Chang, J., "Property of AlN Thin Film on ITO/SiO$_2$ Substrate by Reactive DC Magnetron Sputtering", KIEEME Annual Autumn Conference 2016, Mokpo, Republic of korea, November, 2016.

[6] Kwon, H., **Cho, S.**, Lee, M., Jung, J., & Chang, J., "Property of Microwave Treated Indium-Tin-Oxide Printed Layer", KIEEME Annual Autumn Conference 2016, Mokpo, Republic of korea, November, 2016.

[7] **Cho, S.**, Choi, J., Ko, D., Lee, S., Lee, M., & Chang, J., "Room-temperature growth of AlN on sapphire substrate by Pulse Sputtering Deposition", KIEEME Annual Summer Conference 2017, Pyeongchang, Republic of korea, June, 2017.

[8] Choi, J., Ko, D., **Cho, S.**, Lee, S., & Chang, J., "A Study on the Crystallinity Change of AlN Thin Films grown by Pulsed Sputter Deposition by Annealing", KIEEME Annual Summer Conference 2017, Pyeongchang, Republic of korea, June, 2017.

[9] **Cho, S.**, Cho, Y., Choi, J., Ko, D., Lee, S., Lee, M., & Chang, J., "Optimization of pulsed sputtering deposition conditions of AlN films", The International Workshop on UV Materials and Devices 2017, Fukuoka, Japan, November, 2017.

[10] Ko, D., Choi, J., **Cho, S.**, Cho, Y., Lee, S., & Chang, J., "Electrical properties of AlN films grown by pulsed sputtering deposition", The International Workshop on UV Materials and Devices 2017, Fukuoka, Japan, November, 2017.

[11] **Cho, S.**, Choi, J., Ko, D., Lee, S., Lee, M., & Chang, J., "Influence of sputtering parameters on AlN thin film by Pulse sputter deposition at room temperature", The 4th International Conference on Advanced Electromaterials, Jeju, Republic of korea, November, 2017.

[12] Choi, J., Ko, D., **Cho, S.**, Lee, S., & Chang, J., "Characterization of annealed AlN layers grown by Pulsed Sputter Deposition", The 4th International Conference on Advanced Electromaterials, Jeju, Republic of korea, November, 2017.

[13] Ko, D., Choi, J., **Cho, S.**, Lee, S., & Chang, J., "A study on the capacitance-voltage properties of AlN/Al_2O_3 thin films grown by PSD", The 4th International Conference on Advanced Electromaterials, Jeju, Republic of korea, November, 2017.

Acknowledgement

석사 학위 논문을 마무리까지 많은 사람들의 도움이 있었기에 여기까지 수행할 수 있었습니다. 그 동안 느낀 감사한 마음을 전하고자 합니다.

학부과정부터 석사과정까지 대학생활을 지도해주신 장지호 교수님께 감사한 마음을 전하고 싶습니다. 교수님을 만나게 된 것은 저에게 큰 행운이었습니다. 많이 부족한 저에게 교수님의 말씀들은 표지판과 같았으며, 교수님의 지도 덕분에 많은 성장할 수 있었습니다. 앞으로도 교수님의 말씀들을 잊지 않고 성장하여 사회의 한 축이 되겠습니다.

공동 지도교수이신 선박해양플랜트연구소의 이문진 박사님께도 감사의 말씀 드립니다. 또한 학문적으로도 많은 도움을 주신 전자소재공학전공의 이삼녕, 안형수, 양민, 김홍승, 안지훈 교수님께도 감사드리며, 대학교 생활에 많은 도움을 주신 이봉춘 조교님께도 감사의 말씀을 드립니다.

동고동락한 나노소재연구실의 성국이형, 수훈이형, 석환이형, 준석이, 동완이, 해외에 계신 영지누나와 유진누나 비롯한 많은 선후배님들에게도 감사한 마음을 전합니다. 선후배님들의 많은 도움들 덕분에, 석사 과정 기간은 저에게 보람찬 기간이었습니다. 우리 NMD 선후배님들에게 항상 좋은 일이 가득하길 빌겠습니다.

연구뿐만 아니라 고민들도 함께 교류했던 동기 서영이와 인준이형에게 감사인사를 전합니다. 서로의 연구를 위해 공대 1호관에서 밤낮으로 연구하며, 이제는 미래를 향해 나아가는 두 분 모두 멋있습니다. 석사과정의 연구를 기반으로 대기만성하기 바라겠습니다. 덕분에 힘들 수도 있었던 석사과정이 행복했으며, 많이 웃을 수 있었습니다.

지금은 바쁘다는 평계로 자주 보지 못하는 10학번 창동이형, 영균이, 민석이, 지원이, 동근이, 진이, 지훈이, 현우, 형우, 효대, 희태 이외에도 후배인 지헌이, 다한이, 지호, 종섭이, 권수에게도 감사 인사 전합니다. 지금은 서로 다른 공간에 있어 자주 보지는 못하지만 같이 생활했었던 대학생활은 영원히 간직하겠습니다.

마지막으로 산소 같은 가족들에게 감사한 마음을 전하고 싶습니다.

조용국, 아버지 덕분에 지금까지 올 수 있었으며 석사학위도 무사히 마칠 수 있었습니다. 감사합니다.

이옥남, 어머니 항상 저에게 자신감과 용기를 채워주셔서 감사합니다. 어머니의 은혜 덕분에 무사히 석사학위를 마칠 수 있었습니다. 사랑합니다.

조성우, 세상에서 가장 멋있는 형이 앞에서 이끌어주어서 석사과정을 잘 마무리할 수 있었습니다. 감사합니다.

　여러분들이 주신 감사함에 보답할 수 있는 사람이 되도록 앞으로도 끊임없이 노력하겠습니다.